10706–10727 *Nucleic Acids Research, 2019, Vol. 47, No. 20* *Published online 23 September 2019*
doi: 10.1093/nar/gkz794

PP4 phosphatase cooperates in recombinational DNA repair by enhancing double-strand break end resection

María Teresa Villoria[1], Pilar Gutiérrez-Escribano[2], Esmeralda Alonso-Rodríguez[1], Facundo Ramos[1], Eva Merino[1], Adrián Campos[1], Alex Montoya[3], Holger Kramer[3], Luis Aragón[2] and Andrés Clemente-Blanco[1,*]

[1]Cell Cycle and Genome Stability Group, Institute of Functional Biology and Genomics (IBFG), Spanish National Research Council (CSIC). University of Salamanca (USAL), C/ Zacarías González 2, Salamanca 37007, Spain, [2]Cell Cycle Group. Medical Research Council, London Institute of Medical Science, Du Cane Road, London W12 0NN, UK and [3]Biological Mass Spectrometry and Proteomics Laboratory, Medical Research Council, London Institute of Medical Science, Du Cane Road, London W12 0NN, UK

Received May 09, 2019; Revised August 30, 2019; Editorial Decision September 04, 2019; Accepted September 11, 2019

ABSTRACT

The role of Rad53 in response to a DNA lesion is central for the accurate orchestration of the DNA damage response. Rad53 activation relies on its phosphorylation by Mec1 and its own autophosphorylation in a manner dependent on the adaptor Rad9. While the mechanism behind Rad53 activation has been well documented, less is known about the processes that counteract its activity along the repair of a DNA adduct. Here, we describe that PP4 phosphatase is required to avoid Rad53 hyper-phosphorylation during the repair of a double-strand break, a process that impacts on the phosphorylation status of multiple factors involved in the DNA damage response. PP4-dependent Rad53 dephosphorylation stimulates DNA end resection by relieving the negative effect that Rad9 exerts over the Sgs1/Dna2 exonuclease complex. Consequently, elimination of PP4 activity affects resection and repair by single-strand annealing, defects that are bypassed by reducing Rad53 hyperphosphorylation. These results confirm that Rad53 phosphorylation is controlled by PP4 during the repair of a DNA lesion and demonstrate that the attenuation of its kinase activity during the initial steps of the repair process is essential to efficiently enhance recombinational DNA repair pathways that depend on long-range resection for their success.

INTRODUCTION

Cells are constantly threatened by different sources of DNA damage that can lead to the accumulation of genetic errors that contribute to genome instability. In order to maintain the integrity of the genetic material, cells have developed highly conserved and sophisticated mechanisms that survey their genome, detect DNA lesions and repair them in order to avoid the propagation of mutations. These pathways, collectively known as the DNA damage response (DDR), activate the expression of genes required for DNA repair and trigger checkpoints that inhibit replication and segregation of damaged DNA (1). One of the most hazardous types of DNA lesions is the double-strand break (DSB), produced when the two complementary strands of the double helix are severed simultaneously. DSBs are repaired either by direct ligation of the broken ends, as in non-homologous end joining (NHEJ), or by mechanisms that rely on the searching of homologous sequences to regenerate the original DNA molecule, as DSB repair (DSBR), break-induced replication (BIR) or single-strand annealing (SSA) (2). Homology-dependent DSB repair is always initiated by the nucleolytic degradation of the 5′-ended strand to generate single-stranded DNA (ssDNA), a process known as resection (3). Resection is activated by two sequential events, an initial processing carried out by the MRX complex (Mre11-Rad50-Xrs2) that together with Sae2 produce a short 3′ overhang ssDNA (4) followed by a long-range resection triggered by two redundant pathways involving the Sgs1/Dna2-Top3-Rmi1 complex and the Exo1 nuclease (5,6). Long resection gives rise to extensive ssDNA tracks

*To whom correspondence should be addressed. Tel: +34 923 294 887; Email: andresclemente@usal.es

that are covered by RPA and the DNA damage checkpoint machinery in order to couple the repair process with cell cycle progression (7). In *Saccharomyces cerevisiae*, the DNA damage checkpoint is mainly controlled by the phosphatidyl inositol kinase-like kinase (PIKK) Mec1, the ortholog of ATR in mammals (8). Upon activation, ssDNA-bound Mec1 channels the checkpoint signal to other kinases such as Rad53 or Chk1 (Chk2 and Chk1 in mammals, respectively). These two kinases are responsible for the phosphorylation of multiple downstream targets required for the execution of different biological processes encompassed in the DDR, including a G2/M arrest which allows cells to accomplish the repair of the lesion before re-entry in the division cycle.

Rad53 is involved in multiple and diverse functions along the DNA damage response as replisome stabilization, expression of repair genes, inhibition of late origin firing, suppression of recombination at stalled forks, fork resumption and repair (9). Activation of Rad53 in response to a DNA lesion comprises a complex mechanism that relies on the conserved checkpoint adaptor Rad9, a protein that shares functional and structural properties with three human mediators BRCA1, MDC1 and 53BP1 (10). After generation of a DNA break, Rad9 is associated to damaged chromatin via its BRCT and TUDOR domains, which anchor the protein to Ser129-phosphorylated histone H2A (γH2A) (11). DNA-bound Rad9 is phosphorylated at the DSB vicinity by the cycling-dependent kinase (CDK) (12) and Mec1 (13) to create a specific binding surface for the Rad53-FHA domain (14,15). Recruitment of Rad53 to Rad9 stimulates its phosphorylation by Mec1 to become pre-activated. Besides, Rad53 like other kinases, has the ability to phosphorylate itself. In this regard, it has been proposed that the accumulation of Rad53 at the break site enhances its autophosphorylation and consequently, its full activation (16). Once activated, Rad53 is liberated from the Rad9 complex resulting in the amplification of the checkpoint signal throughout the cell (17).

Even though Rad53 phosphorylation and activation have been extensively studied in the last years, less is known about the mechanisms controlling Rad53 dephosphorylation and inhibition. Interestingly, appearance of unphosphorylated Rad53 after checkpoint inactivation does not require new protein synthesis, suggesting that the activity of the kinase is regulated by dephosphorylation (18). Up to date, a few number of phosphatases have been involved in Rad53 dephosphorylation. Both PP1 and PP2C were described as protein phosphatases necessary to enhance checkpoint inactivation and cell cycle re-entry by targeting Rad53. However, while PP1 is needed during the recovery from HU treatment (19), PP2C is required for cell cycle re-entry upon induction of a DSB (20), suggesting that different phosphatases counteract Rad53 phosphorylation depending on the type of lesion generated. Recently, new data coming from different organisms have demonstrated that protein phosphatase 4 (PP4) is also a key regulator of the DDR. PP4 is an ubiquitous serine/threonine phosphatase that regulates many cellular functions (21). It is composed by the catalytic subunit Pph3 (Ppp4c in mammals) and several regulatory subunits that control the specificity of the holoenzyme. Similarly to PP1 and PP2C, PP4 has the ability to dephosphorylate Rad53, in this case after MMS treatment (22). Interestingly, the role of PP4 in the DNA damage response is not only limited to modulate Rad53 phosphorylation. Dephosphorylation of H2A by PP4 in both yeast and human cells has been linked to an efficient recovery from the DNA damage checkpoint arrest (23–25). Supporting these observations, PP4 was found to regulate many Mec1 targets in response to HU treatment, suggesting that this phosphatase is important to balance the phosphorylation state of multiple substrates in response to replication stress (26). In mammalian cells, PP4 has been implicated in the binding of 53BP1 to chromatin during the formation of a DNA lesion (27) and in promoting cell cycle recovery from the G2/M arrest by dephosphorylating KAP1 (28). Remarkably, the function of PP4 in the DDR is not only restricted to enhance checkpoint inactivation and cell cycle re-entry, but also to repair. In this regard, it has been shown that in the budding yeast, PP4 collaborates with PP2C to stimulate DSB repair by homologous recombination (29). Moreover, experiments in human cells have demonstrated that dephosphorylation of RPA by PP4 facilitates recombinational DNA repair (30). Overall, these results indicate that PP4 has the ability to control multiple aspects of the DNA damage response, including DNA repair, DNA damage checkpoint and cell cycle recovery.

Here, we describe that PP4 is involved in the recombinational repair of DSBs by modulating the steady-state phosphorylation of multiple factors involved in the DNA damage response. This is attained by the ability of the phosphatase to counteract Rad53 phosphorylation during the repair of a DNA lesion. Rad53 attenuation by PP4 enhances DNA end resection by alleviating the negative effect that Rad9 exerts over the Sgs1/Dna2 pathway. Importantly, PP4-dependent resection is crucial for the correct execution of recombinational pathways that rely specifically on the efficiency of the resection process. Accordingly, lack of PP4 activity causes defects in DNA end resection and repair by SSA. Interestingly, both defects are suppressed by reducing the hyperphosphorylation levels of Rad53, demonstrating that Rad53 is the major effector of the phosphatase during the repair of a DNA break. Altogether, we propose that Rad53 inhibition by PP4 is not only restricted to silence the DDR once the DNA lesion has been fixed, but also during the initial steps of the repair process in order to accurately execute recombinational repair pathways that rely on long-range resection for its accomplishment.

MATERIALS AND METHODS

Yeast strains, growing conditions and plasmids

All strains used in this study are listed in Supplementary Table S1. Epitope tagging and gene depletion of endogenous genes were performed by gene targeting using polymerase chain reaction (PCR) products as described in (31) by using the oligonucleotides shown in Supplementary Table S3. For the majority of the experiments cells were grown in YEP containing 2% raffinose. HO expression was attained by adding galactose to a final concentration of 2%. Samples were collected for FACS, DNA and protein analysis before adding galactose and at different time points after the HO induction. The *rad53K227A* mutation was introduced

using an *Eco*RI-linearized pCH3 plasmid (32). All strains containing the *hta1/hta2-S129** versions of H2A were constructed as previously described (33).

Southern blots

Cell lysis was achieved by treating the samples with 40 units of lyticase in DNA preparation buffer (1% SDS, 100 mM NaCl, 50 mM Tris–HCl, 10 mM EDTA) for 10 min. DNA extraction was performed by mixing the samples with phenol:chloroform:isoamylalcohol (25:24:1) for 10 min. After centrifugation, the soluble fraction was precipitated with ethanol and resuspended in TE buffer. Purified DNA was digested with the appropriate restriction enzyme, separated on 0.7–1% agarose gels and subjected to Southern blotting. Probing was performed by labelling a PCR-amplified DNA fragment with a mix of nucleotides containing Fluorescein-12-dUTP (Fluorescein-High Prime, Roche). The oligonucleotides used to synthesize the probes are included in Supplementary Table S2. Detection was attained by using an anti-Fluorescein antibody conjugated with alkaline phosphatase (Anti-Fluorescein-AP Fab fragments, Roche). A FIJI software was used for the processing, analysis and quantification of the images.

Western blots

Samples were prepared by using a trichloroacetic acid (TCA) method. In brief, cells were collected by centrifugation and fixed with 20% TCA. Cells were broken by shaking the pellet with glass beads in a FastPrep machine (MPBio) (3 × 20 s cycles at power setting 5.5). Protein precipitation was reached by centrifugation at 5000 rpm for 5 min at 4°C. Upon precipitation, the pellet was resuspended in 1 M Tris–HCl pH 8 and SDS-PAGE loading buffer, and boiled for 10 min. Insoluble material was separated by centrifugation and the supernatant was loaded in a 6% acrylamide gel. When separating Rad9 phospho-bands, gels were supplemented with 5 μM of Phos-Tag and 10 μM of $MnCl_2$. Proteins were transferred into PVDF membranes (Hybond-P, GE Healthcare) and blocked with 5% milk in PBS-Tween (0.1%). Anti-Rad53 antibody was used at a 1:2000 dilution (Abcam) and the secondary anti-rabbit antibody was used at a concentration of 1:25 000 (GE Healthcare). Anti-HA antibody was used at a 1:2500 dilution (Roche), and the secondary anti-mouse antibody was used at a concentration of 1:25 000 (GE Healthcare). After several washes in PBS-Tween, membranes were incubated with SuperSignal® West Femto (Thermo Scientific), followed by exposure to ECL Hyperfilm (GE Healthcare).

Liquid chromatography-tandem mass spectrometry (LC-MS/MS) analysis

For each sample, 150 ODs of cells were harvested at 4°C, washed once in cold water and frozen at –80°C. Cell pellets were thawed briefly on ice and resuspended in 150 μl of 8 M Urea, 20 mM HEPES pH 8 buffer supplemented with PhosSTOP phosphatase inhibitor tablets (Roche). 300 μl of 425–600 μm glass beads (Sigma) were added and protein extracts were prepared by bead beating using a FastPrep machine (MPBio) at 3 × 30 s pulses and 5.5 power setting. Cell lysates were resuspended in 300 μl of fresh buffer and the soluble fraction was separated from the insoluble fraction by centrifugation at 15 000 rpm for 15 min at 4°C.

For sample processing, 550 μg of protein were reduced and alkylated sequentially with 10 mM dithiothreitol and 50 mM 2-chloroacetamide respectively. Samples were then diluted with 20 mM HEPES buffer (pH 8.0) to 4 M urea and sufficient LysC protease (Wako, 125-05061) was added for a protease to protein ratio of 1:250, followed by incubation (37°C, 5 h). Samples were then diluted to 1 M urea and trypsin (Promega, V5280) was added to a 1:50 ratio for overnight incubation at 37°C. Samples were acidified with trifluoroacetic acid (TFA) to a final concentration of 0.5% prior to solid phase extraction. For total protein analysis, volumes equivalent to 50 μg of protein were de-salted using C18 spin tips (Glygen Corp, TT2C18.96) and peptides eluted with 60% ACN + 0.1% formic acid (FA). Eluents were then dried using a centrifugal vacuum drier. The remaining sample volumes were de-salted using solid phase extraction with OASIS HLB 10 mg cartridges (Waters, 186000383) according to the manufacturer's instructions.

Peptides were eluted from OASIS HLB cartridges with 1 M glycolic acid in 80% acetonitrile (ACN), 5% TFA and phospho-enriched using a TiO_2 based method (34). Briefly, eluents were adjusted to 1 ml with 1 M glycolic acid solution and were then incubated with 25 mg of TiO_2 (50% slurry in 1% TFA) for 5 min at room temperature. After 5 min of incubation with mixing, the TiO_2/peptide mixture was packed into empty spin tips by centrifugation. The TiO_2 layer was then sequentially washed with 1 M glycolic acid solution, 100 mM ammonium acetate in 25% ACN and 10% ACN. Phosphopeptides were eluted with 4 sequential additions of a 5% NH_4OH solution. Eluents were clarified with centrifugation at 13 000 rpm for 2 min and clear supernatant transferred to new tubes. Samples were snap frozen on dry ice and then dried by vacuum centrifugation.

Phospho-enriched samples and desalted total protein digests were redissolved in 0.1% TFA by shaking (1200 rpm) for 30 min and sonication on an ultrasonic water bath for 10 min, followed by centrifugation (14 000 rpm, 5°C) for 10 min. LC-MS/MS analysis was carried out in technical duplicates (1 μg on column for total protein samples) and separation was performed using an Ultimate 3000 RSLC nano liquid chromatography system (Thermo Scientific) coupled to an Orbitrap Velos mass spectrometer (Thermo Scientific) via a Dionex nano-electrospray source. For LC-MS/MS analysis, phosphopeptide solutions were injected and loaded onto a trap column (Acclaim PepMap 100 C18, 100 μm × 2 cm) for desalting and concentration at 8 μl/min in 2% acetonitrile, 0.1% TFA. Peptides were then eluted on-line to an analytical column (Acclaim Pepmap RSLC C18, 75 μm × 50 cm) at a flow rate of 250 nl/min. Peptides were separated using a 120 min gradient, 4–25% of buffer B for 90 min followed by 25–45% buffer B for another 30 min (buffer A: 5% DMSO, 0.1% FA; buffer B: 75% acetonitrile, 5% DMSO, 0.1%FA) and subsequent column conditioning and equilibration. Eluted peptides were analysed by the mass spectrometer operating in positive polarity using a data-dependent acquisition mode. Ions for fragmentation were determined from an initial MS1 survey scan at

30 000 resolution, followed by CID (Collision-Induced Dissociation) of the top 10 most abundant ions. MS1 and MS2 scan AGC targets were set to 1^6 and 3^4 for maximum injection times of 500 ms and 100 ms, respectively. A survey scan m/z range of 350–1500 was used, with multistage activation (MSA) enabled, normalized collision energy set to 35%, charge state screening enabled with +1 charge states rejected and minimal fragmentation trigger signal threshold of 500 counts.

The data was processed using the MaxQuant software platform (v1.6.1.0), with database searches carried out by the in-built Andromeda search engine against the Uniprot *Saccharomyces cerevisiae* database (version 20180305, number of entries: 6729). A reverse decoy database approach was used at a 1% false discovery rate (FDR) for peptide spectrum matches. Search parameters included: maximum missed cleavages set to 2, fixed modification of cysteine carbamidomethylation and variable modifications of methionine oxidation, protein N-terminal acetylation and serine, threonine, tyrosine phosphorylation. For total protein samples, search parameters as above with variable modifications of methionine oxidation, protein N-terminal acetylation, asparagine deamidation and cyclization of N-terminal glutamine to pyroglutamate. Label-free quantification was enabled with an LFQ minimum ratio count of 2. 'Match between runs' function was used with match and alignment time limits of 1 and 20 min respectively.

Chromatin immunoprecipitation assay

For ChIP analysis, 50 ml of culture (at $OD_{600\,nm}$ ≈0.5) were fixed with a final concentration of 1.42% of formaldehyde for 15 min at room temperature. Formaldehyde was quenched with 125 mM glycine for 5 min at room temperature and then harvested by centrifugation at 4000 rpm for 2 min. The pellet was washed with PBS buffer, transferred to a new tube, frozen in liquid nitrogen and stored at −80°C. Cells were re-suspended in 100 μl of IP buffer (150 mM NaCl, 50 mM Tris–HCl, pH 7.5, 5 mM EDTA, NP-40 (0.5% v/v), Triton X-100 (1.0% v/v)) containing 1 mM of phenylmethylsulphonyl fluoride (PMSF), a complete protease inhibitor cocktail (Roche) and 500 μl of glass beads. Cells were lysed by 6 × 20 s cycles on power setting 5.5 in a FastPrep FP120 (BIO 101) machine, with 5 min on ice between cycles. 300 μl of IP buffer containing PMSF and protease inhibitors were then added. Tubes were pierced with a hot needle and placed on top of fresh 1.5 ml tubes and spun at 1000 rpm for 2 min. Samples were centrifuged at 13 000 rpm for 10 min. The nuclear pellet was re-suspended thoroughly and sonicated for 1 h (30 s on, 30 s off at high power at 4°C) (Diagenode Bioruptor). After clarification by centrifuging at 13 000 rpm for 10 min, 100 μl were taken for inputs and 300 μl for the IPs. Inputs were precipitated by adding 0.3 M of potassium acetate and 2.5 volumes of cold ethanol. The mixture was incubated at −20°C for 2 h and spun at 13 000 rpm for 5 min. 250 μl of 10% (w/v) Chelex 100 suspension were added to the dried pellet and boiled for 20 min. The supernatant was cleaned by using a PCR purification kit (GE Healthcare) according to the manufacturer's instructions, and the DNA eluted in 250 μl of water. For IP's treatment, 2 μg of anti-HA antibody (Roche) were added to 300 μl of chromatin and samples were incubated in an ultrasonic water bath for 30 min at 4°C. After clarification by centrifugation at 13 000 rpm for 2 min, the supernatant was added to 25 μl of IP buffer pre-equilibrated Protein A Shepharose beads (GE Healthcare). Sample and beads were incubated for 2 h on a rotating platform at 4°C. The beads were washed five times with IP buffer and added 250 μl of 10% (w/v) Chelex 100. After mixing, the tubes were boiled for 20 min, centrifuged at 13 000 rpm for 1 min and the supernatant was transferred into a fresh tube and stored at −20°C.

Real-time PCR

PCR reactions were performed using the SYBR® Premix Ex Taq™ (Tli RNaseH Plus)(Takara). Reactions were carried out according to the manufacturer's instructions in a total volume of 12 μl containing 3 μl of input or IP DNA and the corresponding pairs of primers (final concentration, 1.5 μM). Amplification was performed in a Bio-Rad C1000 Thermal Cycler in conjunction with the Bio-Rad CFX96 Real-time-system and analysed using CFX manager (Bio-Rad). The primers used for the analysis of an HO break at the *MAT* locus are shown in Supplementary Table S4.

Statistical analysis

All quantifications shown in the article represent the mean ± SD from at least three independent experiments. The data were statistically analysed using a *t*-test and the differences between the strains tested were indicated in the graphs unless otherwise stated ($P < 0.05$*, $P < 0.005$**, $P < 0.0005$***). GraphPad Prism software was used for all statistical analysis.

RESULTS

PP4 is involved in DNA repair by regulating the phosphorylation state of multiple factors of the DNA damage response

As a first approach to determine the role of PP4 in the DNA damage response in *S. cerevisiae*, we verified the effect of different DNA-damaging agents on the growth of cells lacking the catalytic subunit Pph3. Disruption of the *PPH3* gene gave rise to a mild increase in sensitivity to several genotoxic drugs, including the UV-mimic 4-nitroquinoline-1-oxide (4-NQO), the alkylating agent methyl methanesulphonate (MMS) and the radiomimetic drug phleomycin (Supplementary Figure S1A, S1B). The lethality observed in *pph3Δ* cells exposed to all the DNA-damaging agents tested advises for a general role of PP4 in controlling the DNA damage checkpoint and/or DNA repair mechanisms. Interestingly, *pph3Δ* cells were not sensitive to the ribonucleotide reductase inhibitor hydroxyurea (HU), indicating that PP4 activity is not required to maintain cell viability in response to replicative stress (Supplementary Figure S1A, S1B). Even though PP4 was originally described for its role in DNA damage checkpoint deactivation and cell cycle re-entry (22,23,25,35), there are emerging evidences involving the phosphatase in the repair of DNA lesions (24,29,30). To gain insights into a possible role of PP4 in the repair of DSBs, we first monitored the kinetics of SSA/BIR in

the presence or absence of its catalytic subunit Pph3 by using the YMV80 background. This strain contains a 117-base-pair HO-endonuclease recognition sequence within the *LEU2* locus on chromosome III and a 3′ fragment of the *LEU2* gene with homology only to the right end of the break (*U2*) placed 25 kb downstream the HO cut site (Figure 1A) (36). It has been previously shown that this HO-induced DSB is repaired by SSA (36) in a Rad51-independent manner, although it can also be repaired by Rad51-dependent intra-chromosomal BIR (Figure 1A). The HO endonuclease, regulated by the control of a galactose inducible promoter, was expressed in asynchronous cell cultures and samples were taken up to 24 h to determine the efficiency of the repair by Southern blot. Elimination of *PPH3* resulted in a delay in the formation of the repair product compared to wild-type cells (Figure 1B and Supplementary Figure S2A). Correlating with their incapacity to timely repair the DNA lesion, *pph3Δ* cells exhibited a delay in cell cycle re-entry measured by FACS (Figure 1C). Supporting a role for PP4 in DNA repair, cells lacking *PPH3* were slightly more sensitive than the wild-type strain when plated on galactose-containing media (Supplementary Figure S1C). These experiments corroborate that PP4 is necessary for the correct execution of SSA/BIR during the repair of a single induced DSB.

To identify potential targets of PP4 in DNA repair, we performed quantitative phosphoproteomic by mass spectrometry (MS) of samples taken from the experiment described above. Precisely, we screened for variations in the levels of peptide phosphorylation between a wild-type strain and a *pph3Δ* mutant at time 0, 6 and 12 h after expressing the HO endonuclease. As previously shown in Figure 1B, both strains are still lacking a visible repaired product band after 6 h expressing the HO endonuclease. Under this condition, those proteins containing increased phosphorylation levels in the absence of Pph3 will reflect a putative target of the phosphatase directly involved in DNA repair regulation. Twelve hours after the induction of the DSB, both wild-type and *pph3Δ* cells have already repaired the DNA lesion, rendering PP4-dependent phosphorylation changes to a function exclusively associated to cell cycle re-entry. From the 11 974 phosphopeptides detected, we isolated those whose phosphorylation was enriched in the absence of PP4 activity. We found 180 DDR-related proteins with a distinct phosphorylation state between the wild-type and *pph3Δ* mutant. A summary containing the most relevant DNA damage proteins identified is depicted in Figure 1D. Within this group, quantitative comparison between the wild-type and *pph3Δ* strain was applied to classify the discovered targets depending on their averaged phosphorylation across the experimental conditions (Supplementary Figure S3A). Among the potential PP4 substrates isolated were proteins previously characterized as bona-fide targets of the phosphatase, such as RPA (30), histone H2A (23,24) or Rad53 (22,35). It is important to remark that lack of PP4 activity increased phosphorylation of most of these targets by 6 h from the DSB induction, when there was not yet accumulation of the repair product (Figure 1B). This result suggests that PP4 activity might be required to counterbalance the effect of DDR kinases during the restoration of a DNA lesion. Still, we also detected high levels of protein phosphorylation of several DNA damage response proteins in the absence of PP4 activity by 12 h after the induction of the HO break, a time-point where cells have already accomplished the repair process (Figure 1B), likely reflecting its role in checkpoint deactivation and cell cycle re-entry.

Among the targets found, we focused our attention on the central checkpoint kinase Rad53. It has been proposed that Rad53 dephosphorylation by PP4 is needed for efficient cell cycle recovery from MMS treatment (22,35). However, the fact that Rad53 was already hyperphosphorylated during the repair stage prompted us to investigate whether PP4 could be also targeting Rad53 during the repair process. To validate the phosphatase activity of PP4 over Rad53 during the repair pathway, we used Western blotting to follow PP4-dependent changes in Rad53 phosphorylation after inducing a DSB in the YMV80 background used for the MS analysis. Confirming our previous observations, elimination of PP4 activity rendered Rad53 to an increased phosphorylation state when compared to the wild-type strain from 6 h after the generation of the DSB (Figure 1E). Rad53 consists of a central serine/threonine kinase domain, surrounded by two forkhead-associated (FHA) domains (FHA1 and FHA2) (37) and two SQ/TQ cluster regions (SCD1 and SCD2) enriched in Mec1/Tel1-target phosphorylation sites (38). Additionally, Rad53 includes a bipartite NLS domain at the C-terminal region (39) required for its translocation into the nucleus (Figure 1F). To gain insight into the specific PP4-dependent Rad53 dephosphorylation profile, we examined the MS data looking for changes in the phosphorylation pattern of the kinase in both wild-type and *pph3Δ* cells (Figure 1G). We detected 16 residues in the Rad53 sequence that were potentially phosphorylated in response to DNA damage. A summary of the mass spectrometry data for each of these phospho-sites, including their statistical significances, is shown in Supplementary Table S6. A perfect match was found in the phosphorylation profile between a wild-type strain and a *pph3Δ* mutant at T0 (Figure 1G, left panel), with the majority of these sites unphosphorylated except for Ser774, a residue that has been shown to be a target of the Cdk in an unperturbed cell cycle (40). It has been reported that Ser774 phosphorylation does not play any role in the DDR but in morphogenesis (40). As expected, 6 h after the expression of the HO endonuclease, a general increase in the phosphorylation of all phospho-residues was clearly visible in both wild-type and *pph3Δ* strains. However, while a *pph3Δ* mutant presented a maximum level of phosphorylation around the FHA2 domain, wild-type cells displayed a more modest phosphorylation state at this region of the protein (Figure 1G, middle panel). After 12 h from the DSB induction, all phosphorylation sites had been drastically reduced in the wild-type strain whereas *pph3Δ* cells still accumulated high levels of phosphorylation around the FHA2 domain and the NLS (Figure 1G, right panel). Taking into account that phosphorylation of the FHA2 domain has been directly linked to a Rad53 active state (14) and that both FHA2 and NLS have been shown to be auto-Rad53 phosphoryla-

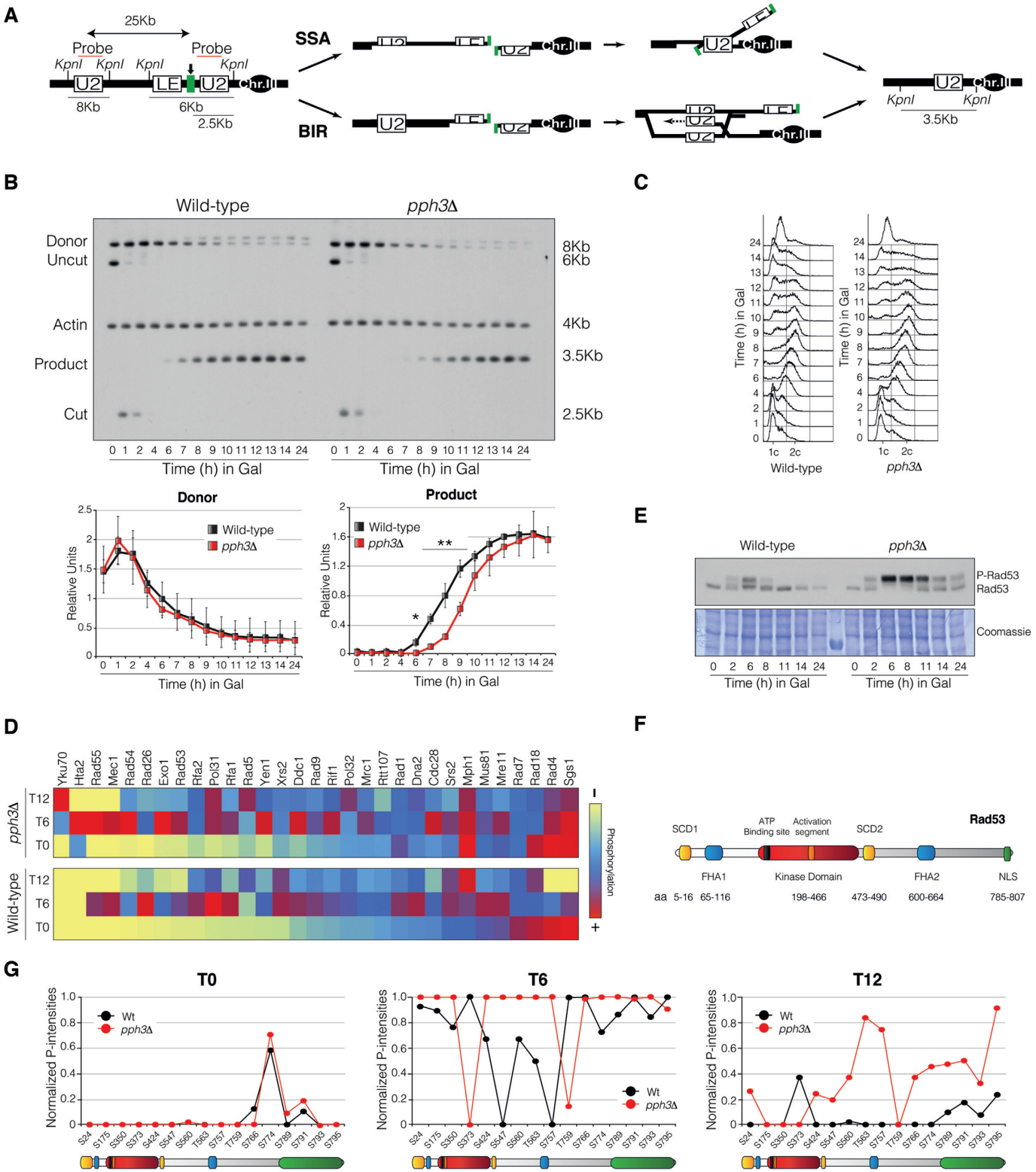

Figure 1. Pph3 is required for DNA repair by homologous recombination by controlling multiple components of the DDR. (**A**) Schematic representation depicting relevant genomic structures of the strain used to assess DNA repair by SSA/BIR. The location of an *U2* probe and the restriction endonuclease cleavage sites used for Southern blot analysis to detect the formation of the repair product are shown. Arrow indicates the localization of the DSB. (**B**) Physical analysis of wild-type and *pph3Δ* mutant strains carrying the DNA repair system depicted in (A). Cells were grown overnight in YP-Raffinose before adding galactose to induce HO expression. Samples were taken at different time points and genomic DNA was extracted, digested with *Kpn*I and analysed by Southern blot. Blots were hybridized with an *U2* and *ACT1* (as loading control) DNA probes. Graphs show the mean ± SD of the band signals from three independent experiments. All data were normalized using actin as loading control. Replicates were averaged and statistical significance of

tion clusters (39,41), these results suggest that PP4 reduces Rad53 activity by counteracting its own autophosphorylation. Overall, these data demonstrate that PP4 is controlling the steady-state phosphorylation of multiple DNA damage factors during the repair of a DNA lesion, possibly by modulating the activity of Rad53 along the process. Importantly, the fact that PP4 activity over Rad53 takes place throughout the repair process indicates that this regulation might be central in the restoration of a DNA lesion.

PP4 is required for DNA end resection

We have previously shown that PP4 activity is required for maintaining a steady-state level of Rad53 phosphorylation in the DDR, a function that is essential to promote an efficient repair by SSA/BIR. It has been proposed that phosphorylation of Exo1 by Rad53 is involved in a negative feedback loop that limits ssDNA accumulation during the resection process (42). On the other hand, Rad9 recruitment to the DSB vicinity depends on Rad53 activity (43). Importantly, Rad9 limits the resection activity of Sgs1/Dna2 by inhibiting the binding of Sgs1 to the DNA lesion (44,45). With all this information, we decided to check whether the hyperphosphorylation levels of Rad53 detected in the absence of PP4 activity could affect SSA/BIR by restraining DNA end resection. To test for a role of PP4 in resection we used a JKM139 derivative strain containing a non-reparable HO system due to the elimination of both *HMR*/*HML* loci (46). As the 5′ strand is degraded, restriction enzymes located at these areas are unable to cleave the generated ssDNA and therefore, the intensity of the bands corresponding to the DNA fragments become diminished (Figure 2A). First, we asked if the activation of a single non-reparable DSB in the absence of Pph3 also increased the levels of Rad53 phosphorylation during the DNA damage response. The fact that the induction of a non-reparable HO cut also led to an hyperphosphorylated Rad53 state confirms that PP4 is acting over Rad53 from the initial steps of the repair process (Figure 2B). To check for resection efficiency, we blocked cells in G1 with alpha factor and released them into new media without the pheromone. One hour later, galactose was added to induce the HO-break (T0), and samples were taken every hour. As expected, while both strains entered the cell cycle and blocked in G2/M with the same kinetics by FACS (Figure 2C), a *pph3Δ* mutant displayed a mild but significant reduction in resection efficiency measured by Southern blot when compared to the wild-type (Figure 2D, E and Supplementary Figure S2B). These experiments suggest that lack of PP4 activity restrains SSA/BIR proficiency by interfering with resection at the DNA lesion.

Reduction of Rad53 phosphorylation levels alleviates PP4-dependent defects in DNA end resection and repair by SSA/BIR

We have shown above that PP4 is specifically targeting the FHA2 domain of Rad53 to restrain its autophosphorylation during the DDR (Figure 1G). Thus, we wondered if the exclusive reduction of Rad53 autophosphorylation might be sufficient to revert the resection defects observed in *pph3Δ* cells. As expected, the substitution of the endogenous RAD53 allele for a kinase dead *rad53K227A* variant in a *pph3Δ* background drastically reduced the high levels of Rad53 phosphorylation observed in a single *pph3Δ* mutant (Figure 3A). This result confirms that the Rad53 hyperphosphorylation observed in the absence of PP4 comes from its own autophosphorylation activity. Importantly, the kinetics of resection in a double *pph3Δ rad53K227A* was slightly increased when compared to a *pph3Δ* control strain (Figure 3B, D and Supplementary Figure S2C), supporting the idea that PP4 counteracts Rad53 autophosphorylation to reduce its inhibitory effect over resection. It is important to remark that a *rad53K227A* strain was fully competent to block in G2/M in response to a single DSB in our experimental conditions (Figure 3C), even though some cells escape from the arrest at late time points, probably due to a failure in the maintenance of the DNA damage checkpoint (47). This rules out a cell cycle-dependent effect in resection activity due to the potential lack of a proficient G2/M arrest when working with the *rad53K227A* variant. We conclude that the effect of PP4 in controlling Rad53 phosphorylation during the initial steps of the repair pathway is directly related to its capacity to modulate resection.

We have previously seen that in the absence of Pph3 the efficiency of DNA repair by SSA/BIR was affected when compared to a wild-type strain. In order to confirm whether this reduction was directly linked to the negative influence that Rad53 hyperactivation exerts over resection, we analysed the effect of reducing Rad53 phospho-levels in *pph3Δ* cells during the execution of SSA/BIR pathways (Figure 3E). Interestingly, Rad53 autoactivation is important for repairing by SSA/BIR, since the substitution of the wild-type version of RAD53 for the *rad53K227A* allele reduced the repair efficiency (Supplementary Figure S4A). Even with this counter-effect, the incorporation of *rad53K227A* into the *pph3Δ* background slightly increased the capacity of the cells to repair a DNA lesion by SSA/BIR when compared to single *pph3Δ* mutants (Figure 3F and Supplementary Figure S2D), and stimulated cell cycle re-entry once the DNA lesion had been restored (Figure 3G). Accordingly, the incorporation of the *rad53K227A* kinase dead version into a *pph3Δ* background slightly improved cell viability on solid media containing MMS or phleomycin (Supple-

←

differences assessed by a two-tailed unpaired Student's t-test. (**C**) FACS profiles of samples taken from (B). (**D**) Samples at 0, 6 and 12 h from the experiment shown in (B) were taken, processed and subjected to mass spectrometry. DDR-related proteins containing at least one phospho-peptide enriched in the absence of PP4 were classified depending on their averaged phosphorylation. Heat map scale represents a $\log_2$ fold change over maximum. Yellow, blue and red indicate relative amount of protein phosphorylation (yellow, low; blue, medium; red, high). (**E**) Samples from the experiment shown in (B) were collected at the indicated time points, proteins TCA extracted and subjected to Western blotting. Coomassie staining is shown as loading control. (**F**) Schematic representation of *S. cerevisiae* Rad53 illustrating the SQ/TQ clusters (yellow), forkhead-associated domains (blue), kinase domain (red) and nuclear localization signal (green). An amino acid residue number scale is shown. (**G**) Graphs representing normalized P-intensities of the Rad53 phospho-peptides identified at 0, 6 and 12 h from the HO induction.

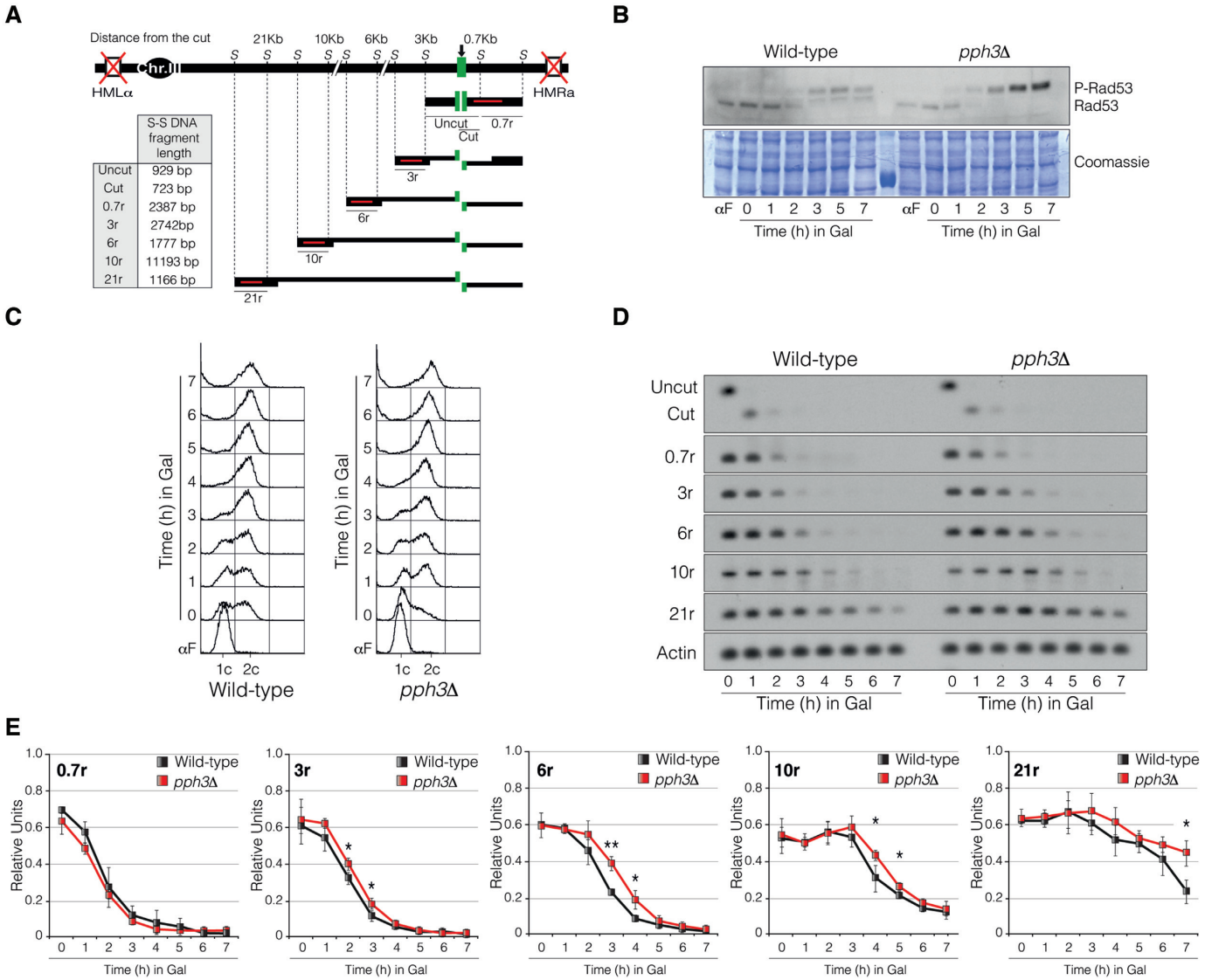

Figure 2. PP4 activity is required to stimulate DNA end resection. (**A**) Schematic representation of the assay used to determine resection efficiency at the *MAT* locus. The diagram includes the recognition sites for *Sty*I and the localization of the probes used (red lines) for each distance. Table includes the *Sty*I-*Sty*I DNA fragments length for each probe. (**B**) Exponentially wild-type and *pph3Δ* cells growing in YP-Raffinose were synchronized in G1 by using the α-factor pheromone and released into fresh media for 1 h. Induction of HO expression was attained by adding galactose to the media and samples were taken at the indicated time points. Proteins were TCA extracted and subjected to Western blotting. Coomassie staining is shown as loading control. (**C**) FACS analysis of the experiment depicted in (B). (**D**) Physical analysis by Southern blot of wild-type and *pph3Δ* strains containing the resection assay described in (A). Samples were taken under the same experimental conditions as in (B), DNA extracted, digested with *Sty*I and blotted. (**E**) Band intensities from the experiment shown in (D) were measured, normalized against actin and plotted. Graphs represent the mean ± SD from three independent experiments. *P*-values were calculated using a two-tailed unpaired Student's t-test.

mentary Figure S1B) supporting the idea of a toxic hyperphosphorylation state of Rad53 in the absence of PP4 activity. Additionally, both *rad53K227A* and *pph3Δ rad53K227A* strains grew similarly on media containing most of the DNA-damaging agents tested, suggesting that both Rad53 and PP4 act in parallel in the same pathway. Besides, there were no apparent differences in the Rad53 phosphorylation status and DNA repair efficiency between a double *pph3Δ rad53K227A* and a single *rad53K227A* (Figure 3E, F and Supplementary Figure S4A), further supporting that PP4 is specifically targeting Rad53 autophosphorylation sites to enhance DNA repair. Thus, we conclude that PP4 participates in DNA repair by counterbalancing Rad53 activity during the initial steps of the DDR in order to trigger a robust resection process that facilitates the execution of the SSA/BIR repair pathways.

PP4-dependent resection is essential for an efficient execution of SSA

As mentioned before, the DSB flanked by direct repeats present in the YMV80 background can be repaired by either SSA or BIR. While SSA repair is strictly dependent on resection for rendering the homologous sequences for an-

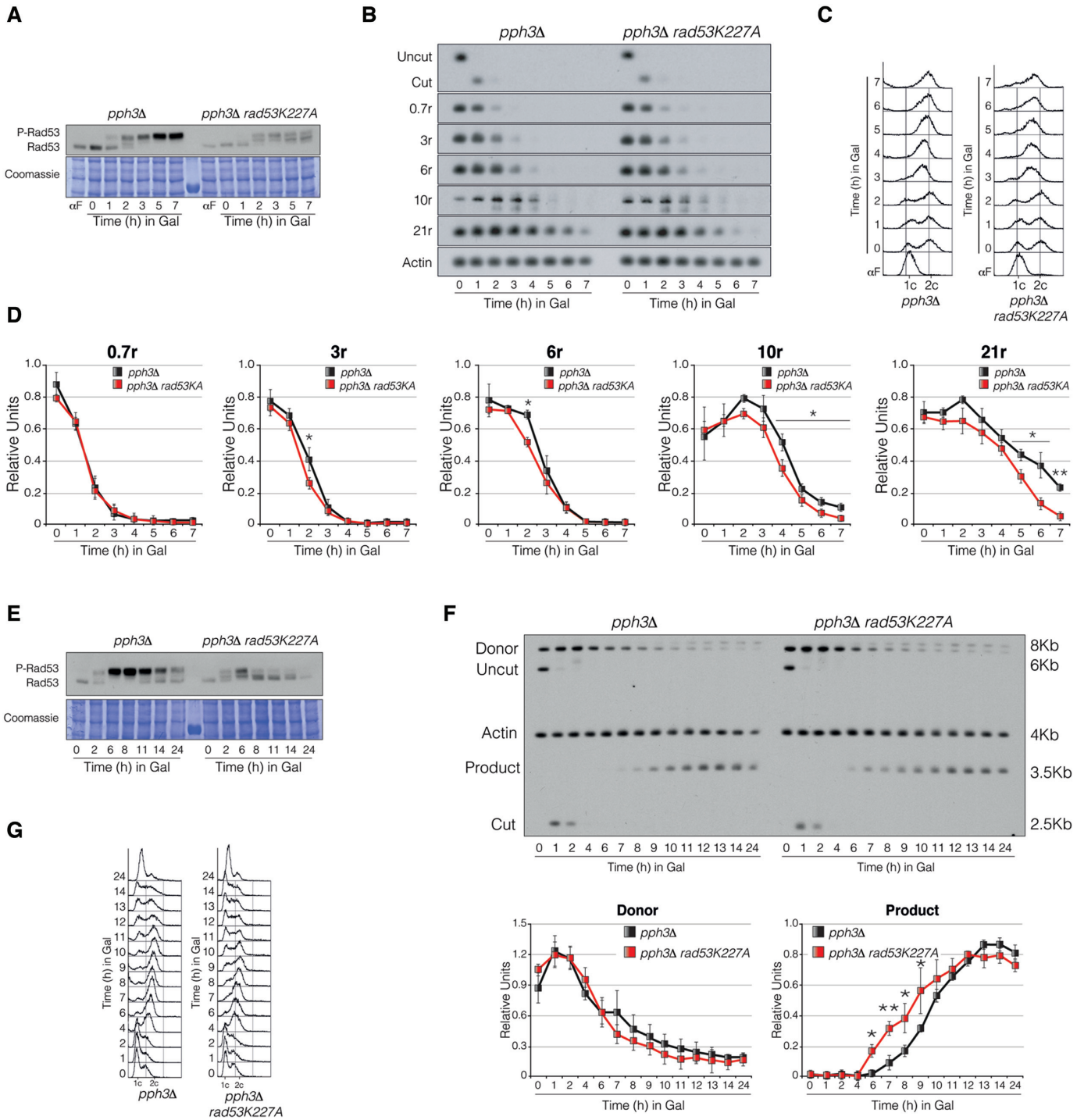

Figure 3. Reduction of Rad53 phospho-levels alleviates PP4-dependent defects in DNA end resection and repair by SSA/BIR. (**A**) Exponentially growing cells from *pph3Δ* and *pph3Δ rad53K227A* backgrounds were synchronized in G1 by using the pheromone α-factor and released into fresh media for 1 h. After inducing the HO expression by adding galactose to the media, samples were collected at the indicated time points and processed for Western blotting. Coomassie staining is shown as loading control. (**B**) Southern blot analysis of samples taken from the experiment shown in (A) to determine resection efficiency. (**C**) FACS analysis of cells collected from (A). (**D**) Band signals from the Southern blot depicted in (B) were quantified, normalized against actin and charted. (**E**) Cells from *pph3Δ* and *pph3Δ* rad53K227A strains were exponentially grown overnight in raffinose-containing media before adding galactose. Samples were collected at the indicated time points and subjected to Western blotting. Coomassie staining is shown as loading control. (**F**) Southern blots of *pph3Δ* and *pph3Δ rad53K227A* cells carrying the DNA repair assay illustrated in Figure 1A. Samples from the experiment shown in (E) were taken at the indicated time points, DNA extracted, digested with *Kpn*I and blotted. Blots were probed with an *U2* DNA sequence and *ACT1* as loading control. Graphs representing the quantification of the band signals from the Southern blot experiment relative to the actin control. (**G**) FACS profile for DNA content of samples collected from the experiment assayed in (F). All graphs in the figure represent the mean ± SD from three independent experiments. P-values were calculated using a two-tailed unpaired Student's t-test.

nealing with each other, BIR involves the formation of a recombination-dependent replication fork to copy all distal sequences. Thus, we wondered whether the defects observed in DNA end resection in the absence of PP4 could affect all types of recombinational DNA repair or, by contrast, might be a process specifically required for repairing by SSA. To check for the involvement of PP4 in inter-chromosomal recombination, we used a genetic background containing a *MATa* sequence at chromosome V that can be recognized by the HO endonuclease and repaired with an uncleavable *MATa-inc* sequence located on chromosome III (48). In this strain, the donor *HM* loci have been eliminated and the *MATa-inc* mutation renders the repair product insensitive to successive HO cleavages (Supplementary Figure S5A). By using this approach, a unique reparable DSB by gene conversion is generated which can occur either with or without an associated crossover (49). As the restriction fragments have an altered size when a crossover is formed, these events can be detected during the repair process. First, we confirmed that Rad53 was also hyperphosphorylated in the absence of PP4 in an inter-chromosomal repair system (Supplementary Figure S5B). Gene conversion with no associated crossover was the predominant form of repair in both wild-type and *pph3Δ* cells. However we could not detect significant differences in the kinetics of DNA repair between both strains (Supplementary Figure S5C, S5D) or in the dynamics of cell cycle re-entry measured by FACS (Supplementary Figure S5E). We neither detected differences in the proportion of gene conversion associated with crossing-over between the wild-type and the *pph3Δ* mutant among cells that repaired the DNA lesion (Supplementary Figure S5C, S5F). These data indicate that PP4 activity is not required to promote ectopic recombination with homologous sequences and suggest that the resection defects observed in the absence of Pph3 exclusively affect DNA repair by SSA.

To further demonstrate this hypothesis, we took advantage of the role of Rad51 in promoting strand annealing. It has been demonstrated that Rad51 is not required for SSA execution but its deletion drastically affects BIR (50). Thus we disrupted *RAD51* in the YMV80 background strain and re-evaluated the effect of PP4 in DNA repair by SSA. Elimination of BIR by depleting Rad51 prolonged Rad53 phosphorylation when compared to a wild-type strain in response to an HO break (Figures 1E and 4A). As expected, a double mutant *rad51Δ pph3Δ* drastically increased Rad53 phospho-levels during the induction of the DSB compared with a single *rad51Δ* mutant (Figure 4A). Correlating with the extended levels of phopho-Rad53 observed in a *rad51Δ* mutant, we monitored a major delay in product accumulation and cell cycle re-entry when comparing to the wild-type strain (Figures 1B, C and 4B, C), probably due to the lack of BIR contribution to the overall kinetics of DSB repair. In agreement with the defect observed in DNA repair efficiency, cell viability of *rad51Δ* single mutants was affected in drop assays on the presence of 4-NQO, HU, MMS and phleomycin (Supplementary Figure S1A, S1B). A similar sensitivity was also observed when the HO-break was induced by plating the cells on galactose-containing media (Supplementary Figure S1C).

Remarkably, a double mutant *rad51Δ pph3Δ* was severely affected in DNA repair by SSA (Figure 4B, C and Supplementary Figure S2E). Interestingly, this defect in the accumulation of the repair product was accompanied by a subtle stabilization of the donor signal. Since the fading of the donor band in the absence of Rad51 depends exclusively on the resection capacity to reach this sequence, this result suggests that PP4 participates in SSA by enhancing DNA end resection. This effect was ratified by using probes located at 10 and 17 kb from the DSB in the same experimental approach. As expected, a double mutant *rad51Δ pph3Δ* mutant resected slower when compared to a *rad51Δ* control strain (Figure 4D), a defect that was more noticeable as longer the distance from the HO was (i.e. 17r). The contribution of PP4 in resection and SSA was supported by a weak synthetic lethality when the *rad51Δ pph3Δ* double mutant was grown on 4-NQO, MMS, phleomycin and galactose (Supplementary Figure S1A–C) and indicates that PP4 acts in a different pathway of Rad51 during the response to DNA damage. However, no effect was observed when combining *rad51Δ* and *pph3Δ* in the sensitivity to HU, again suggesting that PP4 is not involved in the cellular response to replication stress. In all, these results demonstrate that PP4 is particularly necessary for the execution of DNA repair pathways that highly rely on resection to efficiently restore the DNA molecule.

To directly connect the ability of PP4 to counteract Rad53 autophosphorylation with SSA repair, we constructed a *rad51Δ pph3Δ* strain containing the catalytic-dead allele *rad53K227A*. Again, the incorporation of the kinase-dead version of Rad53 reduced the increase in Rad53 phosphorylation levels seen in *rad51Δ pph3Δ* cells (Figure 4E), confirming that PP4 activity counterbalances Rad53 function during DNA repair by SSA. Remarkably, the integration of the *rad53K227A* allele in *rad51Δ pph3Δ* cells considerably improved their ability to repair by SSA (Figure 4F and Supplementary Figure S2F) and thus, their proficiency to re-enter in the cell cycle (Figure 4G). Importantly, these cells also enhanced the disappearance of the donor signal, thus corroborating that high levels of Rad53 phosphorylation restrain SSA execution by interfering with resection. Supporting these data, the incorporation of the *rad53K227A* allele in a double *rad51Δ pph3Δ* background strain partially recovered cell viability in the presence of most of the DNA-damaging agents tested (Supplementary Figure S1B and C). However, only a mild enrichment in SSA efficiency was detected when introducing the *rad53K227A* allele in a *rad51Δ* control strain (Supplementary Figure S4B). Overall, these results support the view that PP4 targets Rad53 to counterbalance its own autophosphorylation, enhance resection and elicit a proficient execution of the SSA repair pathway.

PP4-dependent dephosphorylation of Rad53 enhances DNA end resection mainly by the Sgs1/Dna2 pathway

The helicase activity of Sgs1 is essential for the nuclease Dna2 to degrade the unwound ssDNA in an alternative pathway to the one based on Exo1 (5). Thus we wondered if PP4-dependent activation of resection relies on Dna2 and/or Exo1. To check for a possible function of PP4 in regulating the Exo1 pathway, we generated a single *exo1Δ* and a double *exo1Δ pph3Δ* mutant, and determined their

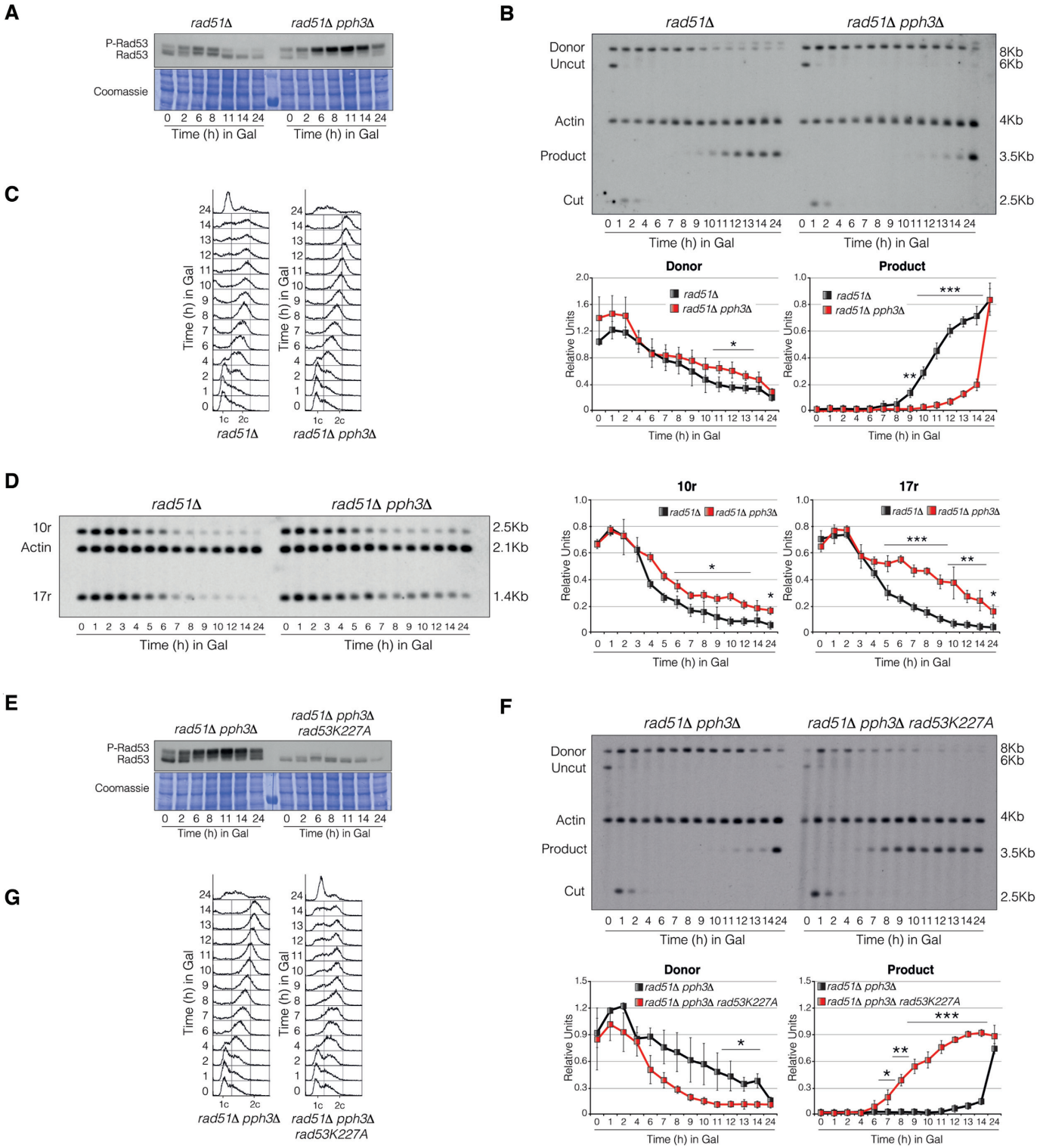

Figure 4. PP4's function in DNA repair becomes essential when repairing by SSA. (**A**) *rad51Δ* and *rad51Δ pph3Δ* cells were grown overnight in raffinose-containing media and supplemented with galactose to induce the expression of the HO. Samples were collected at the indicated time points, proteins TCA extracted and subjected to Western blotting. Coomassie staining is shown as loading control. (**B**) Southern blot analysis of *rad51Δ* and *rad51Δ pph3Δ* strains carrying the DNA repair system depicted in Figure 1A. Samples from the experiment shown in (A) were taken at the indicated time points, genomic DNA extracted, digested with *Kpn*I and analysed by Southern blot. Blots were hybridized with an *U2* and *ACT1* (as loading control) DNA probes. Graphs represent the quantification of the band signals detected in the Southern blot. (**C**) FACS analysis of cells collected from (B). (**D**) *rad51Δ* and *rad51Δ pph3Δ* cells were grown overnight in YP-Raffinose and supplemented with galactose. Samples were taken at different intervals, genomic DNA extracted, digested with *Sty*I and analysed by Southern blot. Blots were hybridized with probes located at 10 kb and 17 kb upstream the HO cut site. Graphs represent the quantification of the band signals detected in the Southern blot. (**E**) Cells from *rad51Δ pph3Δ* and *rad51Δ pph3Δ rad53K227A* background

influence in resection. All strains synchronically exit the alpha factor arrest and block in G2/M with the same kinetic measured by FACS (Figure 5A). The kinetics of DNA resection in an *exo1Δ* mutant was reduced when compared to a *pph3Δ* background. Moreover, lack of Exo1 in a *pph3Δ* mutant exacerbated the resection defect (Figure 5B, C [3r and 6r] and Supplementary Figure S2G). A similar effect was also observed when monitoring the resection intermediates (RI 1–4) generated during the induction of the unrepairable HO-cut (Supplementary Figure S6A). A double *exo1Δ pph3Δ* strain experienced a significant delayed kinetics in the transient appearance of all resection intermediates when compared to a single *exo1Δ* mutant. This effect was more evident when looking at the higher resection intermediates (RI3 and RI4); that is, the longer distances from the break (Supplementary Figure S6A, graphs). It is important to note that elimination of Exo1 did not affect the phosphorylation state of Rad53 (Supplementary Figure S6B), ruling out the possibility of Exo1 acting in the control of resection by interfering with Rad53 phosphorylation. These results demonstrate that the control of PP4 in DNA end resection is mainly carried out independently of Exo1.

To investigate whether PP4 could be modulating the Dna2 resection pathway, we generated single *sgs1Δ* and double *sgs1Δ pph3Δ* mutants and determined their resection capacities. All strains showed a similar FACs profile after being released from the alpha factor arrest (Figure 5D). While a single *sgs1Δ* mutant resected with slower kinetics when compared to a *pph3Δ* mutant, a double *sgs1Δ pph3Δ* resected similarly than a single *sgs1Δ* (Figure 5E, F and Supplementary Figure S2H). The epistasis between *pph3Δ* and s*gs1Δ pph3Δ* in resection was recapitulated by the analysis of the resection intermediates generated during the HO induction (Supplementary Figure S6C). Only a slight defect in RI3-RI4 accumulation was observed between a single *sgs1Δ* and a double *sgs1Δ pph3Δ* mutant, a defect that might be attributed to a minor role of PP4 in controlling the Exo1 pathway. However, the kinetics in the appearance/disappearance of these products was similar between both strains (Supplementary Figure S6C, RI 1–4 graphs), suggesting that the dynamic of resection is not severely exacerbated in PP4-deficent cells lacking Sgs1. As previously reported (51,52), elimination of Sgs1 affects the kinetics of Rad53 phosphorylation (Supplementary Figure S6D), probably due to its defects in DNA end resection and checkpoint activation (51,53). However, lack of Sgs1 did not influence the levels of Rad53 phosphorylation observed in *pph3Δ* cells (Supplementary Figure S6D) indicating that Sgs1 is not acting in the control of resection by interfering with Rad53 phosphorylation in the absence of PP4. These results fit with the idea that PP4 attenuation of Rad53 controls DNA end resection mainly by regulating the activity of the Sgs1/Dna2 route, while a secondary and less robust mechanism comprises the modulation of the Exo1 pathway.

PP4 controls the phosphorylation state of Rad9 by acting over Rad53

We have shown above that Rad53 attenuation by PP4 enhances DNA end resection in a pathway mainly dependent on Sgs1/Dna2. Since it has been established that chromatin-bound Rad9 restrains resection by directly interfering with the activity of the Sgs1/Dna2 pathway (43–45,54), it is intuitive to think that the influence of PP4 over Rad53 could modulate resection by affecting Rad9 phosphorylation. Supporting this hypothesis Rad9 displayed differences in the averaged phosphorylation between a wild-type and a *pph3Δ* mutant in our MS experiment (Figure 1D and Supplementary Figure S3A). Rad9 contains a Chk1 activation domain at the N-terminus (12) close to a Mec1 serine cluster domain. The C-terminus includes a TUDOR domain involved in the binding of Rad9 to the DNA throughout its interaction with H3K79me (55) and a protein-protein recognition module BRCT domain (56) (Figure 6A). We detected 40 residues in Rad9 with the potential to be phosphorylated along with the induction of a reparable HO break. A summary of the mass spectrometry data for each of these phospho-sites, including their statistical significances is included in Supplementary Table S6. An even distribution of Rad9 phospho-peptides alongside the protein was already observed before the induction of the DNA lesion (Figure 6B, top panel). This phosphorylation profile was similar between the wild-type and the *pph3Δ* mutant (Figure 6B, top panel). After 6 h from the induction of the HO endonuclease, a global increase in phosphorylation was observed in both wild-type and *pph3Δ* mutant. However, the absence of PP4 activity specifically increased the phosphorylation levels of several phospho-residues comprised between the serine cluster domain and the TUDOR domain (Figure 6B, middle panel). After 12 h from the HO induction, Rad9 phosphorylation levels decreased in both strains (Figure 6B, bottom panel), indicating that other phosphatases are collaborating with PP4 to reduce Rad9 phosphorylation once the repair process has taken place.

In order to validate these results, we used Phos-Tag gels to follow up PP4-dependent changes in the phosphorylation state of Rad9 after inducing a non-reparable DSB. Ratifying the data obtained by the MS assay, Rad9 was already phosphorylated before the induction of the HO (Figure 6C). However, after inducing the DNA break, we observed an accumulation of higher molecular weight bands that denoted a general hyperphosphorylation state (Figure 6C, first panel). These multiple Rad9 isoforms were predominantly

←

strains were grown overnight in media containing raffinose before adding galactose. Samples were collected at the indicated time points and subjected to Western blotting. Coomassie staining is shown as loading control. **(F)** Southern blot of *rad51Δ pph3Δ* and *rad51Δ pph3Δ rad53K227A* cells carrying the DNA repair system depicted in Figure 1A. Samples from the experiment shown in (E) were taken at the indicated time points, DNA extracted, digested with *Kpn*I and blotted. Blots were hybridized with an *U2* and *ACT1* (as loading control) DNA probes. Graphs represent the quantification of the band signals detected in the Southern blot. **(G)** FACS profile for DNA content of samples collected in (F). All graphs in the figure represent the mean ± SD of the band signals from three independent Southern blot experiments. All data were normalized to actin. Replicates were averaged and statistical significance of differences assessed by a two-tailed unpaired Student's t-test.

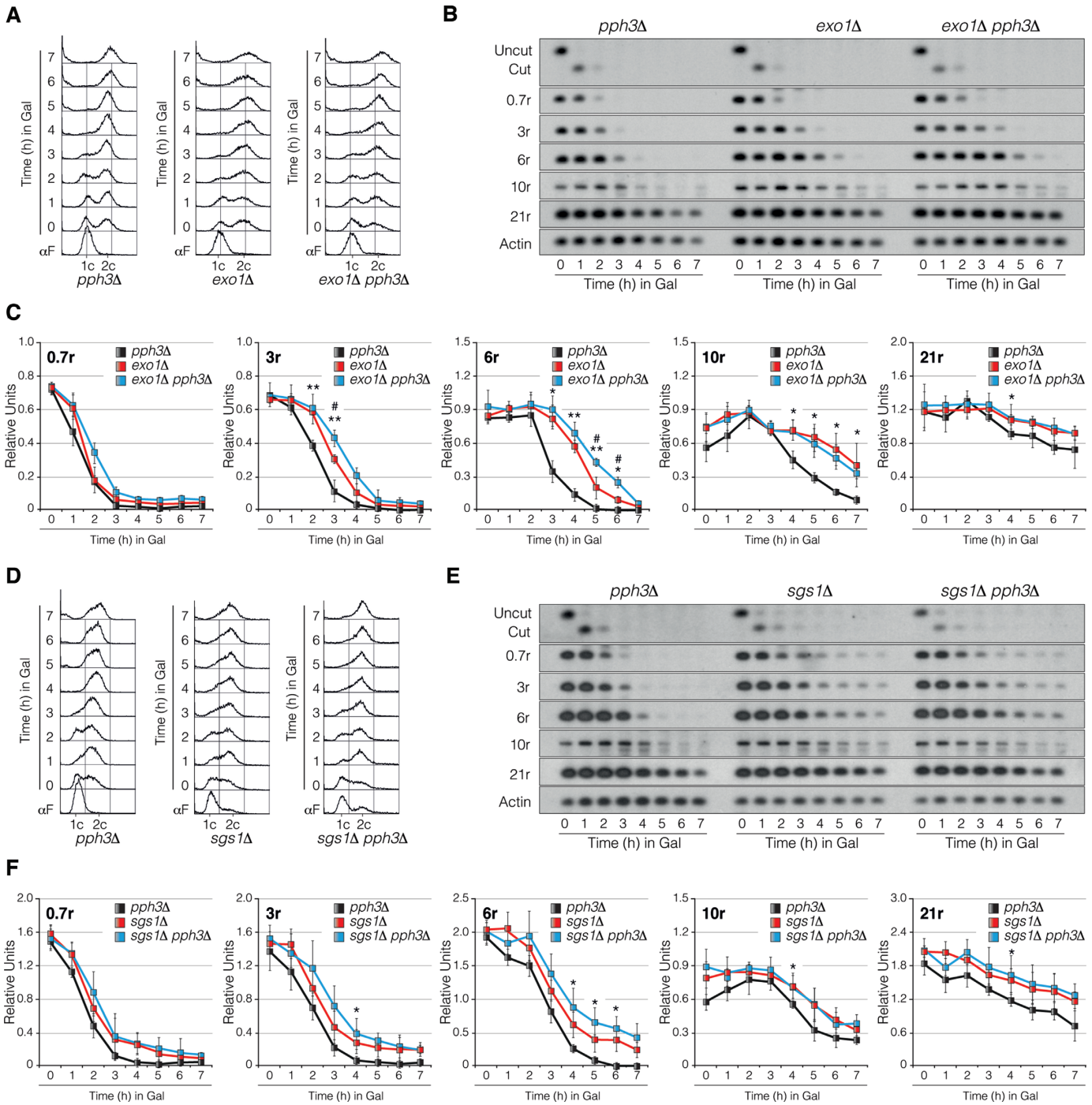

Figure 5. PP4's role in DNA end resection is mainly driven by the modulation of the Sgs1/Dna2 pathway. (**A**) Cultures of *pph3Δ, exo1Δ* and *exo1Δ pph3Δ* cells were grown in YP-Raffinose, blocked in G1 and released into fresh media containing galactose. Cells were collected at the indicated time points and processed for FACS. (**B**) Resection assay by Southern blot of samples taken from (A). Cells were DNA extracted, digested with *Sty*I and blotted. (**C**) The density of the bands depicted in (B) was measured, normalized to actin and plotted. Graphs represent the mean ± SD from three independent experiments. *P*-values were calculated using a two-tailed unpaired Student's *t*-test. Asterisk denotes statistical significance between *pph3Δ* and *exo1Δ* strains. Hash denotes statistical significance between *exo1Δ* and *exo1Δ pph3Δ* strains. (**D**) Cultures of *pph3Δ, sgs1Δ* and *sgs1Δ pph3Δ* cells were cultured in raffinose containing media, arrested in G1 and released into fresh media containing galactose. A FACS profile of cells collected at the indicated time points is represented. (**E**) Resection analysis by Southern blot of samples taken from (D). Cells were DNA extracted, digested with *Sty*I and blotted. (**F**) The intensity of the bands depicted in (E) was measured, normalized to actin and charted. Graphs represent the mean ± SD from three independent experiments. *P*-values were calculated using a two-tailed unpaired Student's t-test. Asterisk denotes statistical significance between *pph3Δ* and *sgs1Δ* strains. Hash denotes statistical significance between *sgs1Δ* and *sgs1Δ pph3Δ* strains.

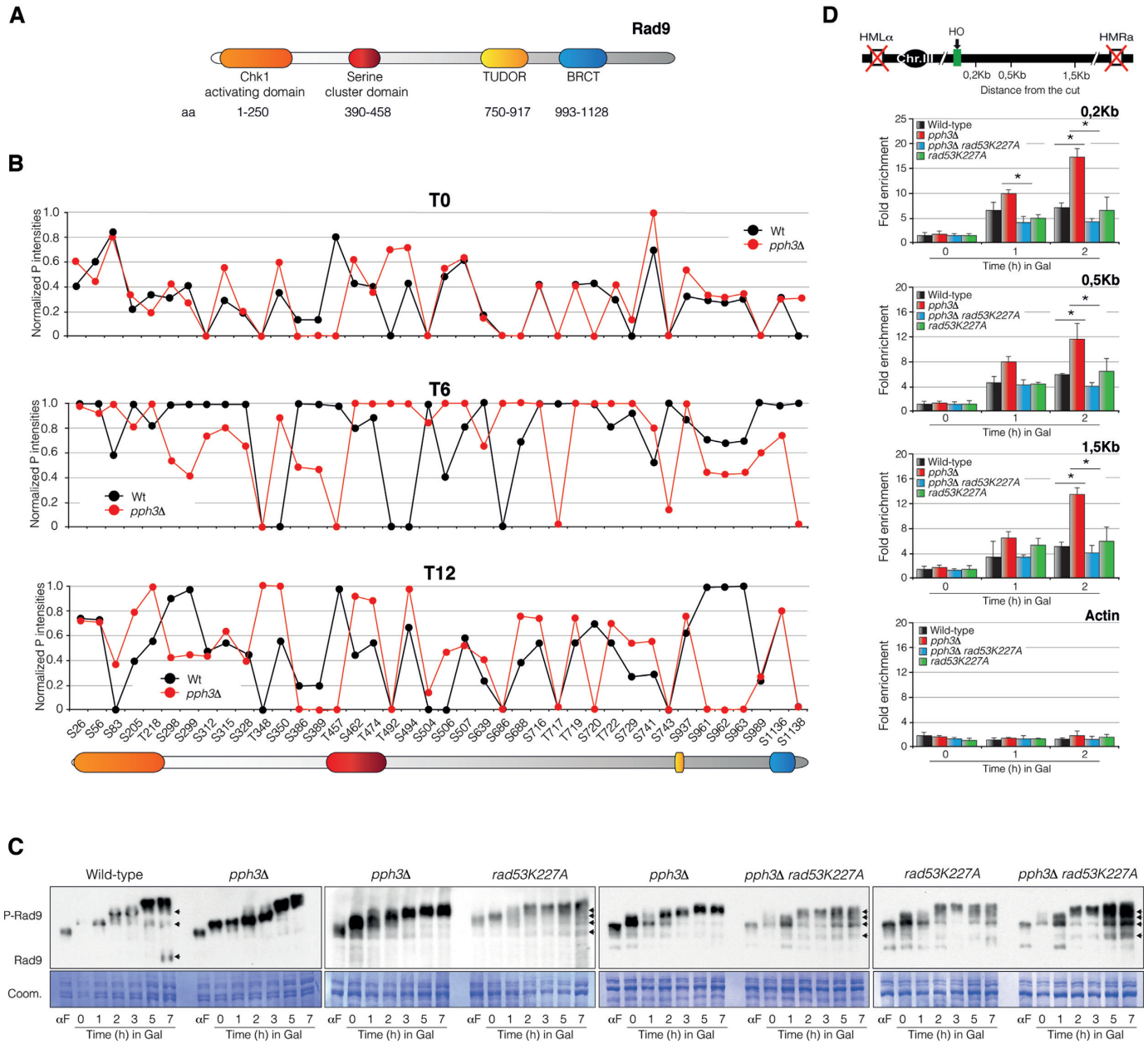

Figure 6. PP4 modulates Rad9 by acting over Rad53. (**A**) Schematic representation of *S. cerevisiae* Rad9 illustrating the Chk1 activating domain (orange), Mec1 serine cluster domain (red), DNA interaction TUDOR domain (yellow) and protein-protein recognition module BRCT domain (blue). An amino acid residue number scale is shown. (**B**) Graphs representing normalized P-intensities of the Rad9 phospho-peptides identified by mass spectrometry at 0, 6 and 12 h from the HO induction. (**C**) Wild-type, *pph3Δ*, *rad53K227A* and *pph3Δ rad53K227A* cells containing the endogenous Rad9 tagged with the HA epitope were subjected to α-factor block and released in the presence of galactose. Samples were blotted using anti-HA antibodies. Coomassie blue staining is depicted as loading control. (**D**) ChIP analysis of Rad9 binding around the HO-induced DSB at the *MAT* locus in wild-type, *pph3Δ*, *pph3Δ rad53K227A* and *rad53K227A* cells. Galactose was added to asynchronous cell cultures and samples were taken at 1 h and 2 h. Each time point was normalized to the input signal. Graphs represent fold enrichment relative to the non-antibody negative control. Binding at the *ACT1* locus on chromosome VI is shown for comparison. Graphs represent the mean ± SD from three independent experiments.

phospho-forms since the treatment with λ-PPase resulted in a drastic reduction in the molecular weight of these bands (Supplementary Figure S3B) only in the absence of phosphatase inhibitors (Supplementary Figure S3C). Interestingly, together with these hyper-phosphorylated bands, a few low molecular weight forms were also detected (Figure 6C, first panel). These fast migrating bands were only detected in the wild-type strain, but not in a *pph3Δ* strain (Figure 6C, first panel), suggesting that lack of PP4 activity affects the phosphorylation status of Rad9. Substitution of the endogenous *RAD53* for the *rad53K227A* allele reduced Rad9 phosphorylation when compared to *pph3Δ* cells (Figure 6C, second panel). Moreover, the introduction of the *rad53K227A* variant overcame the high levels of Rad9 phosphorylation observed in cells lacking PP4 activity (Figure 6C, third panel). These results confirm that Rad53 kinase

activity is important to enhance a proficient Rad9 activation in response to DNA damage. Interestingly, a similar pattern of Rad9 phospho-forms distribution was observed between a *rad53K227A* and a *pph3Δ rad53K227A* strain (Figure 6C, fourth panel), suggesting that the Rad9 hyperphosphorylation state observed in the absence of PP4 activity was Rad53-dependent.

Our data suggest that PP4 restrains Rad9 phosphorylation by acting over Rad53 in response to a DNA lesion (Figure 6C). In addition, we have shown that depletion of *PPH3* increases Rad9 phosphorylation at the vicinity of its TUDOR domain (Figure 6B). Considering that this region is responsible for Rad9 binding to chromatin (55) and that Rad9 association to a DNA break depends on Rad53 activity (43), it seems that Rad53 hyperactivation in the absence of PP4 activity might affect DNA resection by enhancing Rad9 affinity for the DNA lesion. To check for this hypothesis we performed chromatin immunoprecipitation experiments of Rad9 in wild-type and *pph3Δ* cells. As expected, a robust increase in the amount of Rad9 bound at 0.2, 0.5 and 1.5 kb from the HO break was observed in *pph3Δ* when compared to wild-type (Figure 6D). Interestingly, the high levels of Rad9 association to the HO site in the absence of PP4 activity were drastically reduced in *pph3Δ* cells containing the *rad53K227A* variant (Figure 6D). As previously reported (43), a single *rad53K227A* strain displayed a very mild effect in Rad9 binding to the DSB vicinity when compared to the wild-type (Figure 6D). These results confirm that PP4-dependent Rad53 inhibition during the initial steps of the repair process is required to reduce Rad9 association to the DNA lesion, thus diminishing the negative effect that this factor exerts over resection by the Sgs1/Dna2 pathway.

Disruption of Rad9 bypasses the lack of PP4 activity in DNA end resection and repair

Our previous data indicate that PP4 counteracts Rad53 autophosphorylation along the DDR to avoid excessive phosphorylation of the Sgs1/Dna2 inhibitor Rad9. If Rad9 hyperactivation in the absence of PP4 activity is the final event that restrains resection, we speculated that elimination of Rad9 should bypass *pph3Δ* deficiencies in DNA end resection and repair. To confirm this hypothesis, we analysed the resection efficiency of a single *pph3Δ* mutant and in combination with a *RAD9* deletion. As expected, the kinetics of DNA resection in *pph3Δ rad9Δ* cells is markedly increased when compared to *pph3Δ* cells, indicating that *rad9Δ* suppresses the resection defect caused by the lack of Pph3 (Figure 7A, D and Supplementary Figure S2I). Importantly, both *pph3Δ rad9Δ* and *rad9Δ* cells behave similarly in resection (Supplementary Figure S7A) and survival assays to genotoxic agents (Supplementary Figure S1A) suggesting that both proteins act in the same pathway of the DNA damage response. It is important to note that due to the role of Rad9 in DNA damage checkpoint activation (57), a double mutant *pph3Δ rad9Δ* is not able to completely block in G2/M after the induction of the HO break (Figure 7B) and cells notably reduce Rad53 phosphorylation when compared to a single *pph3Δ* strain (Figure 7C).

To determine whether the improvement in resection observed in the double mutant *pph3Δ rad9Δ* was enough to recover the DNA repair defects observed in the single *pph3Δ* mutant, we compared SSA/BIR proficiency in the YMV80 background between both strains. Correlating with the improvement in DNA end resection observed in a double *pph3Δ rad9Δ* mutant, we detected a significant increase in the efficiency of DSB repair (Figure 7E and Supplementary Figure S2J) and cells re-entered in the cell cycle faster than a single *pph3Δ* mutant (Figure 7F). Accordingly, the lethality observed in *pph3Δ* cells growing on solid media containing 4-NQO, MMS, phleomycin and galactose was partially relieved by ablating *RAD9* (Supplementary Figure S1A, S1C). Moreover, *PPH3* deletion in *rad9Δ* cells neither exacerbated repair by BIR/SSA (Supplementary Figure S9A) nor sensitivity to genotoxic stress (Supplementary Figure S1A, C) when compared to cells lacking *RAD9*, indicating that Pph3 exclusively acts in the Rad9 pathway. It is important to note that while a double mutant *pph3Δ rad9Δ* retained some Rad53 phosphorylation (Figure 7G), a single *rad9Δ* strain completely abolished its phosphorylation (Supplementary Figure S8A), suggesting that in the absence of Rad9, Rad53 retains certain capacity to be phosphorylated, but this phosphorylation is eliminated by the activity of PP4 during the DNA damage response. Moreover, a *rad9Δ* single mutant repaired more efficiently and re-entered in the cell cycle with faster kinetics than the wild-type strain (Supplementary Figure S8A) confirming that Rad9 has a general effect in restraining SSA/BIR execution.

To confirm that the effect of PP4 over SSA was dependent on its ability to trigger DNA end resection, we determined the repair efficiency of the YMV80 background in a double *rad51Δ pph3Δ* and triple *rad51Δ pph3Δ rad9Δ* mutants. As expected, disruption of *RAD9* in a *rad51Δ pph3Δ* mutant completely restored SSA efficiency (Figure 7H and Supplementary Figure S2K) and cells re-entered the cell cycle with a faster kinetics than the control strain (Figure 7I). To avoid any cell cycle interference in the repair proficiency due to the lack of DNA damage checkpoint activity inherent in the *rad9Δ* strain, we evaluated DNA repair in alpha factor pre-synchronized G1 cells released into YP-galactose media containing nocodazole to avoid mitotic entry. Under these conditions, a triple *rad51Δ pph3Δ rad9Δ* mutant was still recovering the product signal more efficiently than a double *rad51Δ pph3Δ,* ruling out a cell cycle-dependent effect in the repair of the HO break due to the lack of Rad9 activity (Supplementary Figure S9B). This improvement in DNA repair was also corroborated by the increase in cell viability observed in the triple *rad51Δ pph3Δ rad9Δ* mutant compared to the double *rad51Δ pph3Δ* mutant on solid media containing 4-NQO, MMS, phleomycin and galactose (Supplementary Figure S1A, C). Likewise, elimination of *PPH3* in a *rad51Δ rad9Δ* strain neither exacerbated DNA repair by SSA (Supplementary Figure S9C) nor cell sensitivity to DNA-damaging agents (Supplementary Figure S1A, C), demonstrating that Pph3 and Rad9 work in the same pathway. Importantly, deletion of *RAD9* in a *rad51Δ* background also improved SSA efficiency and cell cycle re-entry (Supplementary Figure S8B), suggesting that the defects in SSA observed in the absence of Rad51 are directly linked to the negative effect that Rad9

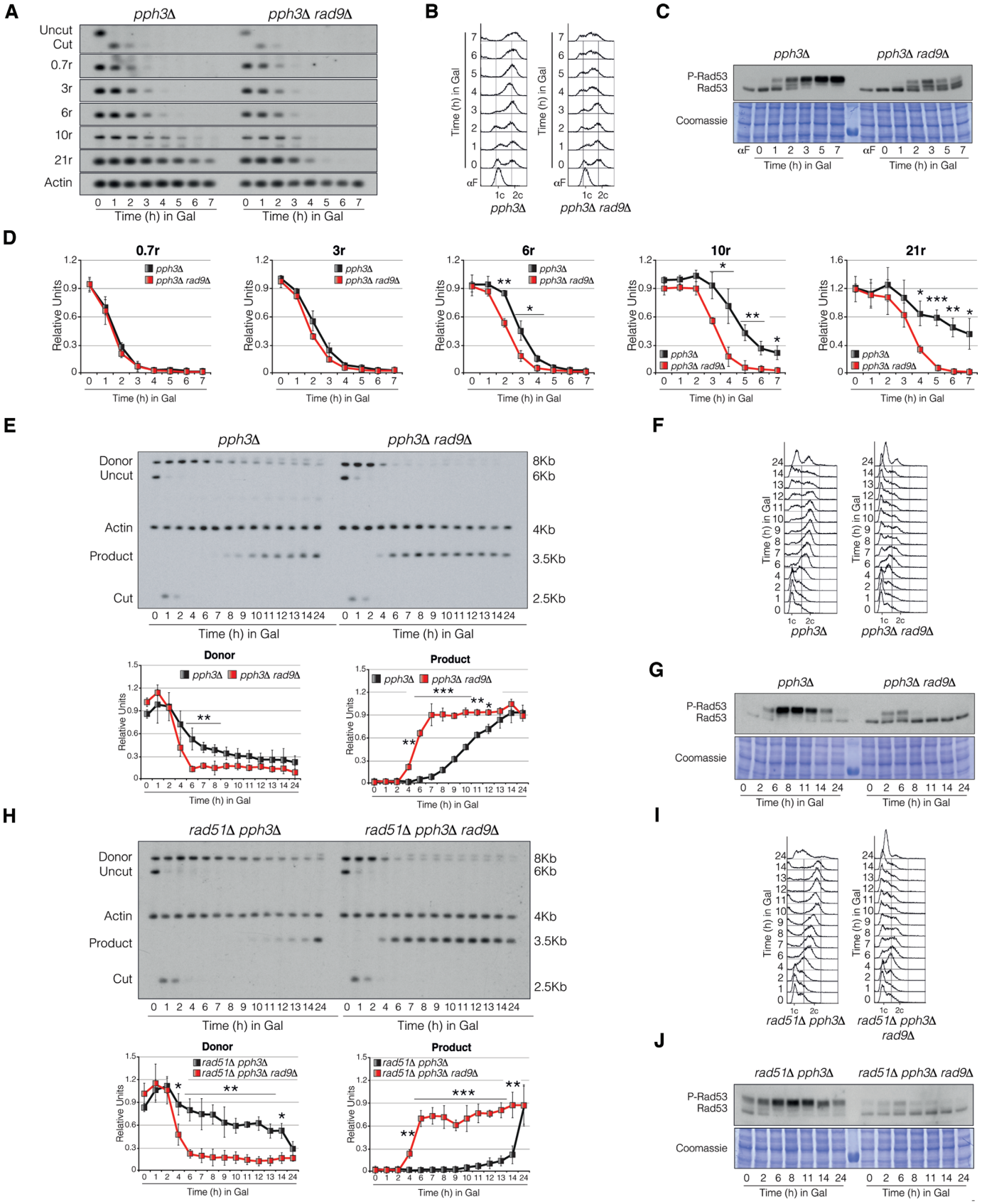

Figure 7. Disruption of Rad9 bypasses the resection and SSA repair defects observed in the absence of PP4 activity. (**A**) Exponentially growing cells of *pph3Δ* and *pph3Δ rad9Δ* strains were synchronized in G1 by using α-factor and released into fresh media for 1 h. After inducing the HO expression by

exerts over resection. Importantly, depletion of Rad9 in a *rad51Δ pph3Δ* strain drastically reduced Rad53 phosphorylation (Figure 7J) nearly to wild-type levels (Figure 1E). However, while a *rad51Δ pph3Δ rad9Δ* triple mutant retained certain capacity to phosphorylate Rad53 (Figure 7J), a double *rad51Δ rad9Δ* completely abolished its phosphorylation (Supplementary Figure S8B), indicating that PP4 is actively dephosphorylating Rad53 during the repair of the DNA lesion to enhance SSA repair.

The defects in DNA end resection and repair observed in PP4-deficient cells are bypassed by restraining Rad9 binding to the DNA lesion

We have previously shown that Rad9 disruption bypassed all defects observed in cells lacking PP4 activity suggesting that Rad9 is the final effector of the PP4/Rad53 module. However, since elimination of Rad9 reduces Rad53 phosphorylation (Figure 7C, G, J) (14) we cannot discard indirect effects due to the low levels of checkpoint activation reached in these strains. It has been postulated that Rad9-dependent inhibition of Sgs1/Dna2 is attained by its physical interaction at the DSB vicinity, a process that depends on Rad53 (43) and phosphorylation of histone H2A at Ser129 (11,58). Importantly, PP4 inactivation increased Rad9 phosphorylation specifically at its TUDOR domain (Figure 6B) and enhanced its binding to the vicinity of the DSB (Figure 6D) indicating that PP4-dependent Rad53 regulation is vital to avoid excessive loading of Rad9 to the DNA break. Thus, we decided to determine whether elimination of Ser129 phosphorylation of H2A, and thus Rad9 binding to the DSB, bypasses all phenotypes observed in the absence of PP4 activity. We constructed a strain in which Ser129 of H2A was substituted by a stop codon in both *HTA1* and *HTA2* alleles (*hta1/hta2-S129**) (33) and determined its influence in rescuing both DNA end resection and SSA/BIR repair defects observed in cells lacking Pph3. First, we checked if the substitution of the *HTA1/HTA2* alleles with the *hta1/hta2-S129** versions was able to reduce the affinity of Rad9 to a DNA break. As previously observed, lack of PP4 activity increases the levels of Rad9 at the vicinity of the DSB (Figure 8A). These high levels of Rad9 binding to the HO vicinity in the absence of *PPH3* were drastically reduced when introducing the *hta1/hta2-S129** constructs (Figure 8A) confirming that these histones variants are not fully competent to tether Rad9 to chromatin. Still, this residual Rad9 binding was capable to retain a modest capacity to restrain resection and product accumulation since the elimination of *RAD9* in *hta1/hta2-S129** cells slightly affects both resection and repair by SSA/BIR (Supplementary Figure S10A). Interestingly, elimination of Ser129 from H2A in a *pph3Δ* background did not affect Rad53 activation when compared with a *pph3Δ* mutant in response to a DSB (Figure 8B). However, these cells considerably increased the repair efficiency by SSA/BIR (Figure 8C top panel, D and Supplementary Figure S2L) and re-entered in the cell cycle with faster kinetics (Figure 8E). Since Rad53 phosphorylation was triggered with the same efficiently in both *pph3Δ* and *pph3Δ hta1/hta2-S129**, this result confirms that the high levels of Rad53 phosphorylation observed in the absence of PP4 are specifically modulating Rad9 capacity to interact with H2A phosphorylated at Ser129. Strikingly, a double mutant *pph3Δ hta1/hta2-S129** resected faster than a single *pph3Δ,* corroborating that the improvement in DNA repair is directly linked to its ability to stimulate DNA resection (Figure 8C bottom panel and F) due to elimination of the negative effect that Rad9 exerts over the Sgs1/Dna2 pathway.

DISCUSSION

Phosphorylation in response to DNA damage has been one of the main subjects in the field of DNA repair, focusing mainly in the regulation of the kinases operating in the DDR. Even though there is a consensus agreement that dephosphorylation is essential for restoring the effects imposed by the DDR-kinases, less is known about the role of protein phosphatases during the execution of the DNA damage response. To date, most of the functions attributed to the DDR-phosphatases during the response to a DNA lesion have been related to their capacity to inactivate the DNA damage checkpoint and promote cell cycle re-entry. However, taking into account the great complexity of the different pathways encompassed in the DDR and the multiple events taking place during the repair of a DNA adduct, it is tempting to speculate that the fine-tuning phosphorylation along the different steps of the repair process might be essential to ensure the restoration of the DNA molecule. In agreement with this hypothesis, we report here a model whereby Rad53 dephosphorylation by PP4 during the initial stages of the repair pathway stimulates DNA end resection, a feature that enhances DSB repair. The maintenance of a reduced Rad53 activity ensures a low steady-state phos-

←

adding galactose to the media samples were collected at the indicated time points and subjected to a resection analysis by Southern blotting. (**B**) FACS profile of cells collected from (A). (**C**) Samples from (A) were taken at the indicated time points and subjected to Western blotting. Coomassie staining is shown as loading control. **(D)** Bands from the Southern blot depicted in (A) were quantified, normalized against actin and plotted. (**E**) Physical analysis of *pph3Δ* and *pph3Δ rad9Δ* cells harbouring the DNA repair assay portrayed in Figure 1A. Cells were grown in YP-Raffinose and transferred to media supplemented with galactose. Samples were collected at different time points, genomic DNA extracted, digested with *Kpn*I and analysed by Southern blot. Blots were hybridized with an *U2* and *ACT1* (as loading control) DNA probes. Graphs show the quantification of the band signals relative to actin. (**F**) FACS profile for DNA content of samples taken from (E). (**G**) Samples from the experiment shown in (E) were collected at the indicated time points, TCA extracted and subjected to Western blotting. Coomassie staining is shown as loading control. (**H**) Physical analysis of *rad51Δ pph3Δ* and *rad51Δ pph3Δ rad9Δ* backgrounds harbouring the DNA repair assay portrayed in Figure 1A. Cells were grown overnight in YP-Raffinose and supplemented with galactose. Samples were taken at different time points, genomic DNA extracted, digested with *Kpn*I and analysed by Southern blot. Blots were hybridized with an *U2* and *ACT1* (as loading control) DNA probes. Graphs represent the quantification of the band signals relative to actin. (**I**) FACS profile for DNA content of samples collected from (H). (**J**) Samples from the experiment shown in (H) were collected at the indicated time points, TCA extracted and subjected to Western blotting. Coomassie staining is shown as loading control. All graphs in the figure represent the mean ± SD from three independent experiments. Replicates were averaged and statistical significance of differences assessed by a two-tailed unpaired Student's t-test.

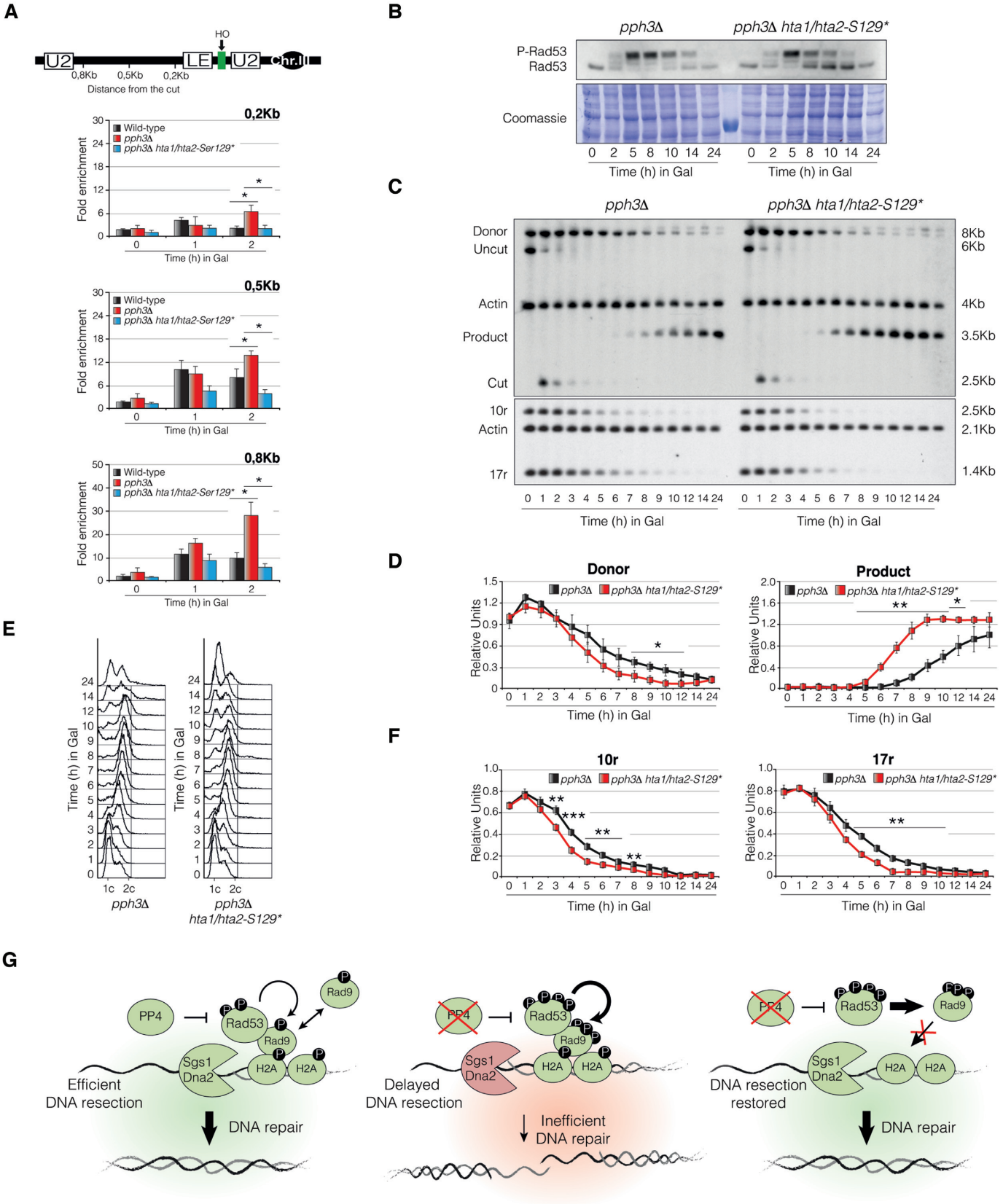

Figure 8. Elimination of H2A phosphorylation at Ser129 rescues both DNA end resection and repair defects of cells lacking PP4 activity. (**A**) ChIP analysis of Rad9 binding around the HO-induced DSB at the *LEU2* locus in wild-type, *pph3Δ*, and *pph3Δ hta1/hta2-S129** cells. Each time point was normalized to the input signal. Graphs represent fold enrichment relative to the non-antibody negative control. (**B**) YP-Raffinose cell cultures of YMV80 derivative

phorylation of multiple targets during the response, including Rad9. Reduction in Rad9 phosphorylation counteracts its inhibitory function over the Sgs1/Dna2 complex by reducing its affinity to chromatin, ensuring a robust and efficient resection activation needed for repair mechanisms that rely on long ssDNA trails to ensure the success of the repair (Figure 8G, left panel). In cells lacking PP4 activity, the high levels of Rad53 activity lead to a hyperphosphorylated state of Rad9, enhancing its binding to the DSB vicinity and restraining resection by Sgs1/Dna2 (Figure 8G, middle panel). Importantly, Sgs1/Dna2-dependent resection defects observed in the absence of PP4 activity are bypassed by just reducing Rad9 binding to chromatin. This indicates that Rad53 down-regulation by PP4 controls resection by preventing the recruitment of Rad9 to the DSB vicinity (Figure 8G, right panel). Importantly, this model implies that excessive checkpoint activation is not compatible with DNA repair pathways that depend on long-range resection for their accomplishment and envisions that DDR kinases and phosphatases must cooperate along the damage response to couple checkpoint activation with DNA repair. This balance in checkpoint activation ensures a precise DNA damage response, strong enough to activate an accurate G2/M cell cycle arrest but not too robust to negatively influence in the repair of the DNA lesion.

Interestingly, MS data of cells lacking PP4 activity revealed an elevated number of DNA damage factors other than Rad53 and Rad9 with atypical high levels of phosphorylation along the damage response. Taking into account that PP4 exhibited a preference for dephosphorylating Rad53 autophosphorylation sites suggests that the modulation of its kinase activity could influence the steady-state phosphorylation of multiple downstream DDR targets. Still, we cannot discard that PP4 might also collaborate in the direct dephosphorylation of Rad53's targets during the response to a DNA lesion. However, the fact that some of the targets found to be hyperphosphorylated in the absence of PP4 activity restored their phosphorylation levels when inhibiting Rad53 autophosphorylation claims for a main role of the phosphatase in directly controlling the phosphorylation status of the kinase. It is important to note that PP4 might also be controlling Rad53 activity by modulating the phosphorylation/activity of upstream kinases. In this regard, it has been recently shown that the absence of Mec1-S1991 phosphorylation in *mec1-100* cells is restored upon *PPH3* deletion, indicating that PP4 indeed dephosphorylates Mec1 (26). However, phosphorylation of this residue requires also the activity of Rad53 (26), suggesting that PP4 might be indirectly affecting Mec1 phosphorylation throughout the modulation of Rad53 activity. Moreover, we could not detect differences in Mec1 phosphorylation between wild-type and PP4-deficienct cells in our MS data during the induction of an HO-break, indicating that PP4 has not an important role in controlling Mec1 phosphorylation in our experimental conditions.

An important question that arises from these observations is how Rad53 hyperphosphorylation in the absence of *PPH3* influences the repair process. Our data show that PP4 is required for an optimal DNA resection by reducing Rad53 phosphorylation levels, a mechanism that has been previously demonstrated to negative influence the activity of the pathway. Importantly, a double mutant *pph3Δ exo1Δ* was significantly more affected in resection than single *pph3Δ* or *exo1Δ* mutants, suggesting that PP4 contribution over Exo1 is not the main mechanism controlling resection. In agreement with this observation, it has been reported that changing Exo1 phospho-residues to alanines or glutamic acids (to prevent or mimic phosphorylation, respectively), has a subtle effect on Exo1 processivity (42) indicating that the activity of this exonuclease is not controlled by its steady-state phosphorylation levels. Still, we cannot discard a possible function of PP4 in directly dephosphorylating Exo1 along the repair of a DNA lesion. Interestingly, combination of *pph3Δ* with *sgs1Δ* only slightly exacerbated the resection problems observed in the single mutants, suggesting that PP4-dependent Rad53 dephosphorylation predominantly affects Sgs1/Dna2 activity. It has been previously described that Rad9 provides a barrier to resection through limiting the association of Sgs1 to the DSB ends (44,45). Curiously, Rad9 association to the DSB vicinity depends on Rad53 kinase activity (43). Taking into account that we observed an increased Rad53-dependent phosphorylation of Rad9 in the absence of PP4 activity, it is tempting to speculate that Rad53 dephosphorylation by PP4 enhances Sgs1/Dna2-dependent resection by reducing Rad9 phosphorylation. Nevertheless, we cannot discard that PP4 might also be directly targeting Rad9 in order to reduce its negative effect on resection during the DNA damage response.

How does the PP4/Rad53 module operate in the regulation of Rad9 association to damaged DNA? It has been previously reported that Rad9 binding to a DNA lesion depends specifically on H2A phosphorylation at Ser129 (11). Chromatin-bound Rad9 is phosphorylated by Mec1 (13) to activate the recruitment of Rad53 to the DSB, an interaction that triggers its autophosphorylation activity (16). It has been reported in both human and yeasts that Rad9 binds to a DNA damaged site throughout its TUDOR domain (55,59). Taking into account that Rad9 hyperphos-

←

pph3Δ and *pph3Δ hta1/hta2-S129** cells were supplemented with galactose to induce the HO expression and samples were collected at the indicated time points. Proteins were TCA extracted and subjected to Western blotting. Coomassie staining is shown as loading control. (**C**) Physical analysis of *pph3Δ* and *pph3Δ hta1/hta2-S129** cells harbouring the DNA repair assay portrayed in Figure 1A. Samples from the experiment shown in (B) were taken at different time points, genomic DNA extracted, digested with *Kpn*I (DNA repair) or *Sty*I (resection) and analysed by Southern blot. Blots were hybridized with an *U2* probe to determine DNA repair efficiency (top panel) and with probes located at 10 kb and 17 kb upstream the HO cut site for the analysis of resection (bottom panel). In both cases *ACT1* was used as loading control. (**D**) Graphs represent the quantification of the donor and product band signals obtained from the Southern blot experiment shown in (C, top panel) relative to the actin signal. (**E**) FACS profile for DNA content of samples collected in (C). (**F**) Graphs represent the quantification of the 10r and 17r band signals obtained from the Southern blot experiment shown in (C, bottom panel) relative to the actin signal. (**G**) Model to integrate the role of PP4 in DSB repair. All graphs in the figure represent the mean ± SD from three independent experiments. Replicates were averaged and statistical significance of differences assessed by a two-tailed unpaired Student's t-test.

phorylation in the absence of PP4 was mainly accumulated around its TUDOR domain, it is reasonable to propose that hyperactive Rad53 enhances Rad9 binding to chromatin, thus creating a positive feedback loop that ends up with the hyperactivation of the DNA damage checkpoint. In line with this hypothesis cells lacking *PPH3* displayed a Rad53-dependent increase in Rad9 loading into a HO-induced DNA break. This suggests that PP4 activity over Rad53 is required to relax the interaction of Rad9 to damaged DNA, thus overcoming the negative effect that this factor exerts over the Sgs1/Dna2 pathway. This model fits perfectly well with the observation that elimination of Ser129 from H2A is sufficient to rescue both the DNA resection and repair phenotypes of cells lacking PP4 activity.

Even though Rad53-dependent Rad9 phosphorylation could constitute a perfect mechanism to explain the link between PP4 and resection, we cannot discard that other targets of the phosphatase could be regulating the binding of Rad9 to the DNA lesion. In fact, it has been reported that the direct dephosphorylation of H2A by PP4 regulates not only cell cycle recovery (23,25) but also DNA repair (24,29). Curiously, we found that H2A phosphorylation was indeed increased in the absence of PP4 activity in our MS screening during the repair of a DNA lesion. This result corroborates previous observations demonstrating that H2A is hyperphosphorylated in cells lacking PP4 activity in response to MMS treatment (29). Taking into account that H2A phosphorylation is a prerequisite to recruit Rad9 to a DSB, it is feasible to think that the direct dephosphorylation of H2A by PP4 could be part of an additional mechanism that regulates Rad9 interaction to the DNA lesion. Besides, Sgs1 phosphorylation by Mec1 has been implicated in the recruitment of Rad53 to damaged sites (51). Therefore, we cannot discard that PP4 could also have a role in Rad9 regulation by acting over Sgs1. Accordingly, we also detected high levels of Sgs1 phosphorylation in the absence of PP4 activity in our mass spectrometry analysis. Whether the direct regulation of these targets by PP4 constitutes additional mechanisms to modulate the steady-state activity of the resection process is a fascinating question for the future.

Another interesting subject to focus on is how does PP4-dependent Rad53 dephosphorylation affect cell cycle resumption upon repair. Interestingly, while PP4 has been previously reported to have a role in DNA damage recovery when cells are treated with MMS (22), we did not observe a clear defect in cell cycle re-entry upon repair of a unique HO break. There are two non-mutually exclusive interpretations to explain this apparent controversy. One possibility is that PP4-dependent checkpoint deactivation depends on the extent of the damage infringed and/or the type of genotoxic stress. Accordingly, Pph3 is dispensable for Rad53 recovery after replication stress (60). Moreover, the activity of Rad53 during MMS recovery is quite similar between wild-type and *pph3Δ* cells, indicating that Rad53 phosphorylation and kinase activity can be separated (60). Another possibility to explain the lack of an evident cell cycle re-entry defect in the absence of PP4 during the induction of a reparable DSB is that other phosphatases might compensate the loss of PP4 during recovery. In this regard, it has been proposed that only the combination of *pph3Δ* with *ptc2Δ* and *ptc3Δ* restrains cells to deactivate Rad53 and resume the cell cycle (60).

In addition to the molecular details behind PP4 regulation of the DDR, it is also important to focus our attention into the physiological significance of this phosphatase in controlling DNA end resection and its implications in DNA repair. Our data using an inter-chromosomal DSB repair approach mediated by gene conversion demonstrate that lack of PP4 activity does not influence DNA repair by ectopic recombination. This result confirms previous observations indicating that only the simultaneous depletion of PP4 and PP2C activities affects DNA repair through DSBR (29). As HR by gene conversion has been demonstrated to require limited amount of ssDNA (5,6,61) it is possible that PP4-dependent resection might be crucial for the repair of DSBs that rely on long-range resection. Accordingly, we have shown that PP4 activity becomes essential when cells are forced to use SSA as the unique pathway to restore a DSB. What is the benefit to support SSA by promoting long-range resection? Resection is activated in S phase through the increasing activity of the CDK, a mechanism that bias DNA repair towards HR even in the absence of the replicated chromatid. Thus, a DSB that occurs in S phase prior sister chromatid synthesis relies exclusively on SSA for its repair (62). In this context, repair by SSA might be critical for cell viability in response to DNA damage. It is important to remark that SSA is especially important in higher eukaryotes, whose genomes are enriched in DNA repeats. In this regard, it has been speculated that an inefficient resection in the absence of PP4 could lead to an excessive initiation of homologous recombination pathways that increase the accumulation of DNA intermediates and rearrangements between repeats, a feature that has been proven to increase genome heterozygosis (63). Additionally, it has been demonstrated that reliance on SSA could compensate genetic deficiencies in HR pathways, as the BRCA2 mutation associated with breast/ovarian cancer (64).

DATA AVAILABILITY

The mass spectrometry proteomics data have been deposited to the ProteomeXchange Consortium via the PRIDE partner repository database (http://www.ebi.ac.uk/pride) with the data set identifier PXD013782. The data uploaded in the repository contain the results from two independent biological experiments. Each biological duplicate was subjected to two technical replicate (TR). Samples processed to isolate phospho-peptides (PE) and total protein (TP) are included. A table containing the nomenclature for each file generated during the analysis is shown in the supplementary material section (Supplementary Table S5).

SUPPLEMENTARY DATA

Supplementary Data are available at NAR Online.

ACKNOWLEDGEMENTS

We would like to thank P. San Segundo and J. Haber for providing valuable strains and plasmids. We particularly thank

Vincent Géli, Jessica A. Downs and J.A. Tercero for providing plasmids. We are grateful to O. Calvo for her support with the chromatin immunoprecipitation experiments. We thank P. San Segundo, CR. Vazquez de Aldana and J. Correa for helpful comments, discussions and reading of the manuscript.

Author contributions: A.C.-B. planned and evaluated most experiment. M.T.V. was responsible for the development of the majority of the experiments reported in the paper. P.G.E. and L.A. were responsible for the mass spectrometry experiments. A.M. and H.K. were responsible for performing the mass spectrometry analysis. E.A-R, F.R., E.M. and A.C. provided technical support to this work. A.C.-B. wrote the paper and all authors analysed the data, discussed the results and commented on the manuscript.

FUNDING

Ministerio de Economía y Competitividad [BFU2013-41216-P, BFU2016-77081-P and PGC2018-097963-B-100 (MCIU/AEI/FEDER, UE) granted to A.C.-B.]; The IBFG is supported in part by an institutional grant from the 'Junta y Castilla y León' (Programa 'Escalera de Excelencia' de la Junta de Castilla y León, Ref. CLU-2017-03 cofinanciado por el P.O. FEDER de Castilla y León 14–20); M.T.V. was recipient of a predoctoral fellowship from the 'Junta de Castilla y León'; F.R. was recipient of a predoctoral fellowship from the 'Ministerio de Economía y Competitividad'. Funding for open access charge: Ministerio de Economía y Competitividad Grand [Reference 1: BFU2016-77081-P, Grand Reference 2: PGC2018-097963-B-100].

Conflict of interest statement. None declared.

REFERENCES

1. Harper,J.W. and Elledge,S.J. (2007) The DNA damage response: ten years after. *Mol. Cell*, **28**, 739–745.
2. Symington,L.S., Rothstein,R. and Lisby,M. (2014) Mechanisms and regulation of mitotic recombination in Saccharomyces cerevisiae. *Genetics*, **198**, 795–835.
3. Mimitou,E.P. and Symington,L.S. (2009) DNA end resection: many nucleases make light work. *DNA Repair (Amst.)*, **8**, 983–995.
4. Gobbini,E., Cassani,C., Villa,M., Bonetti,D. and Longhese,M.P. (2016) Functions and regulation of the MRX complex at DNA double-strand breaks. *Microb. Cell*, **3**, 329–337.
5. Zhu,Z., Chung,W.H., Shim,E.Y., Lee,S.E. and Ira,G. (2008) Sgs1 helicase and two nucleases Dna2 and Exo1 resect DNA double-strand break ends. *Cell*, **134**, 981–994.
6. Mimitou,E.P. and Symington,L.S. (2008) Sae2, Exo1 and Sgs1 collaborate in DNA double-strand break processing. *Nature*, **455**, 770–774.
7. Ciccia,A. and Elledge,S.J. (2010) The DNA damage response: making it safe to play with knives. *Mol. Cell*, **40**, 179–204.
8. Durocher,D. and Jackson,S.P. (2001) DNA-PK, ATM and ATR as sensors of DNA damage: variations on a theme? *Curr. Opin. Cell Biol.*, **13**, 225–231.
9. Branzei,D. and Foiani,M. (2006) The Rad53 signal transduction pathway: replication fork stabilization, DNA repair, and adaptation. *Exp. Cell Res.*, **312**, 2654–2659.
10. Zhou,B.B. and Elledge,S.J. (2000) The DNA damage response: putting checkpoints in perspective. *Nature*, **408**, 433–439.
11. Hammet,A., Magill,C., Heierhorst,J. and Jackson,S.P. (2007) Rad9 BRCT domain interaction with phosphorylated H2AX regulates the G1 checkpoint in budding yeast. *EMBO Rep.*, **8**, 851–857.
12. Abreu,C.M., Kumar,R., Hamilton,D., Dawdy,A.W., Creavin,K., Eivers,S., Finn,K., Balsbaugh,J.L., O'Connor,R., Kiely,P.A. *et al.* (2013) Site-specific phosphorylation of the DNA damage response mediator rad9 by cyclin-dependent kinases regulates activation of checkpoint kinase 1. *PLos Genet.*, **9**, e1003310.
13. Schwartz,M.F., Duong,J.K., Sun,Z., Morrow,J.S., Pradhan,D. and Stern,D.F. (2002) Rad9 phosphorylation sites couple Rad53 to the Saccharomyces cerevisiae DNA damage checkpoint. *Mol. Cell*, **9**, 1055–1065.
14. Sweeney,F.D., Yang,F., Chi,A., Shabanowitz,J., Hunt,D.F. and Durocher,D. (2005) Saccharomyces cerevisiae Rad9 acts as a Mec1 adaptor to allow Rad53 activation. *Curr. Biol.*, **15**, 1364–1375.
15. Sun,Z., Hsiao,J., Fay,D.S. and Stern,D.F. (1998) Rad53 FHA domain associated with phosphorylated Rad9 in the DNA damage checkpoint. *Science*, **281**, 272–274.
16. Pellicioli,A. and Foiani,M. (2005) Signal transduction: how rad53 kinase is activated. *Curr. Biol.*, **15**, R769–R771.
17. Gilbert,C.S., Green,C.M. and Lowndes,N.F. (2001) Budding yeast Rad9 is an ATP-dependent Rad53 activating machine. *Mol. Cell*, **8**, 129–136.
18. Tercero,J.A., Longhese,M.P. and Diffley,J.F. (2003) A central role for DNA replication forks in checkpoint activation and response. *Mol. Cell*, **11**, 1323–1336.
19. Bazzi,M., Mantiero,D., Trovesi,C., Lucchini,G. and Longhese,M.P. (2010) Dephosphorylation of gamma H2A by Glc7/protein phosphatase 1 promotes recovery from inhibition of DNA replication. *Mol. Cell Biol.*, **30**, 131–145.
20. Leroy,C., Lee,S.E., Vaze,M.B., Ochsenbein,F., Guerois,R., Haber,J.E. and Marsolier-Kergoat,M.C. (2003) PP2C phosphatases Ptc2 and Ptc3 are required for DNA checkpoint inactivation after a double-strand break. *Mol. Cell*, **11**, 827–835.
21. Cohen,P.T., Philp,A. and Vazquez-Martin,C. (2005) Protein phosphatase 4–from obscurity to vital functions. *FEBS Lett.*, **579**, 3278–3286.
22. O'Neill,B.M., Szyjka,S.J., Lis,E.T., Bailey,A.O., Yates,J.R. 3rd, Aparicio,O.M. and Romesberg,F.E. (2007) Pph3-Psy2 is a phosphatase complex required for Rad53 dephosphorylation and replication fork restart during recovery from DNA damage. *Proc. Natl. Acad. Sci. U.S.A.*, **104**, 9290–9295.
23. Keogh,M.C., Kim,J.A., Downey,M., Fillingham,J., Chowdhury,D., Harrison,J.C., Onishi,M., Datta,N., Galicia,S., Emili,A. *et al.* (2006) A phosphatase complex that dephosphorylates gammaH2AX regulates DNA damage checkpoint recovery. *Nature*, **439**, 497–501.
24. Chowdhury,D., Xu,X., Zhong,X., Ahmed,F., Zhong,J., Liao,J., Dykxhoorn,D.M., Weinstock,D.M., Pfeifer,G.P. and Lieberman,J. (2008) A PP4-phosphatase complex dephosphorylates gamma-H2AX generated during DNA replication. *Mol. Cell*, **31**, 33–46.
25. Nakada,S., Chen,G.I., Gingras,A.C. and Durocher,D. (2008) PP4 is a gamma H2AX phosphatase required for recovery from the DNA damage checkpoint. *EMBO Rep.*, **9**, 1019–1026.
26. Hustedt,N., Seeber,A., Sack,R., Tsai-Pflugfelder,M., Bhullar,B., Vlaming,H., van Leeuwen,F., Guenole,A., van Attikum,H., Srivas,R. *et al.* (2015) Yeast PP4 interacts with ATR homolog Ddc2-Mec1 and regulates checkpoint signaling. *Mol. Cell*, **57**, 273–289.
27. Lee,D.H., Acharya,S.S., Kwon,M., Drane,P., Guan,Y., Adelmant,G., Kalev,P., Shah,J., Pellman,D., Marto,J.A. *et al.* (2014) Dephosphorylation enables the recruitment of 53BP1 to double-strand DNA breaks. *Mol. Cell*, **54**, 512–525.
28. Lee,D.H., Goodarzi,A.A., Adelmant,G.O., Pan,Y., Jeggo,P.A., Marto,J.A. and Chowdhury,D. (2012) Phosphoproteomic analysis reveals that PP4 dephosphorylates KAP-1 impacting the DNA damage response. *EMBO J.*, **31**, 2403–2415.
29. Kim,J.A., Hicks,W.M., Li,J., Tay,S.Y. and Haber,J.E. (2011) Protein phosphatases pph3, ptc2, and ptc3 play redundant roles in DNA double-strand break repair by homologous recombination. *Mol. Cell Biol.*, **31**, 507–516.
30. Lee,D.H., Pan,Y., Kanner,S., Sung,P., Borowiec,J.A. and Chowdhury,D. (2010) A PP4 phosphatase complex dephosphorylates RPA2 to facilitate DNA repair via homologous recombination. *Nat. Struct. Mol. Biol.*, **17**, 365–372.
31. Janke,C., Magiera,M.M., Rathfelder,N., Taxis,C., Reber,S., Maekawa,H., Moreno-Borchart,A., Doenges,G., Schwob,E., Schiebel,E. *et al.* (2004) A versatile toolbox for PCR-based tagging of yeast genes: new fluorescent proteins, more markers and promoter substitution cassettes. *Yeast*, **21**, 947–962.

32. Pellicioli,A., Lucca,C., Liberi,G., Marini,F., Lopes,M., Plevani,P., Romano,A., Fiore,Di and Foiani,M. (1999) Activation of Rad53 kinase in response to DNA damage and its effect in modulating phosphorylation of the lagging strand DNA polymerase. *EMBO J.*, **18**, 6561–6572.
33. Downs,J.A., Lowndes,N.F. and Jackson,S.P. (2000) A role for Saccharomyces cerevisiae histone H2A in DNA repair. *Nature*, **408**, 1001–1004.
34. Casado,P., Bilanges,B., Rajeeve,V., Vanhaesebroeck,B. and Cutillas,P.R. (2014) Environmental stress affects the activity of metabolic and growth factor signaling networks and induces autophagy markers in MCF7 breast cancer cells. *Mol. Cell. Proteomics : MCP*, **13**, 836–848.
35. Szyjka,S.J., Aparicio,J.G., Viggiani,C.J., Knott,S., Xu,W., Tavare,S. and Aparicio,O.M. (2008) Rad53 regulates replication fork restart after DNA damage in Saccharomyces cerevisiae. *Genes Dev.*, **22**, 1906–1920.
36. Jain,S., Sugawara,N., Lydeard,J., Vaze,M., Gac,Tanguy Le and Haber,J.E. (2009) A recombination execution checkpoint regulates the choice of homologous recombination pathway during DNA double-strand break repair. *Genes Dev.*, **23**, 291–303.
37. Durocher,D., Henckel,J., Fersht,A.R. and Jackson,S.P. (1999) The FHA domain is a modular phosphopeptide recognition motif. *Mol. Cell*, **4**, 387–394.
38. Traven,A. and Heierhorst,J. (2005) SQ/TQ cluster domains: concentrated ATM/ATR kinase phosphorylation site regions in DNA-damage-response proteins. *Bioessays*, **27**, 397–407.
39. Smolka,M.B., Albuquerque,C.P., Chen,S.H., Schmidt,K.H., Wei,X.X., Kolodner,R.D. and Zhou,H. (2005) Dynamic changes in protein-protein interaction and protein phosphorylation probed with amine-reactive isotope tag. *Mol. Cell. Proteomics : MCP*, **4**, 1358–1369.
40. Diani,L., Colombelli,C., Nachimuthu,B.T., Donnianni,R., Plevani,P., Muzi-Falconi,M. and Pellicioli,A. (2009) Saccharomyces CDK1 phosphorylates Rad53 kinase in metaphase, influencing cellular morphogenesis. *J. Biol. Chem.*, **284**, 32627–32634.
41. Chen,E.S., Hoch,N.C., Wang,S.C., Pellicioli,A., Heierhorst,J. and Tsai,M.D. (2014) Use of quantitative mass spectrometric analysis to elucidate the mechanisms of phospho-priming and auto-activation of the checkpoint kinase Rad53 in vivo. *Mol. Cell. Proteomics : MCP*, **13**, 551–565.
42. Morin,I., Ngo,H.P., Greenall,A., Zubko,M.K., Morrice,N. and Lydall,D. (2008) Checkpoint-dependent phosphorylation of Exo1 modulates the DNA damage response. *EMBO J.*, **27**, 2400–2410.
43. Gobbini,E., Villa,M., Gnugnoli,M., Menin,L., Clerici,M. and Longhese,M.P. (2015) Sae2 function at DNA Double-Strand breaks is bypassed by dampening tel1 or Rad53 activity. *PLos Genet.*, **11**, e1005685.
44. Bonetti,D., Villa,M., Gobbini,E., Cassani,C., Tedeschi,G. and Longhese,M.P. (2015) Escape of Sgs1 from Rad9 inhibition reduces the requirement for Sae2 and functional MRX in DNA end resection. *EMBO Rep.*, **16**, 351–361.
45. Ferrari,M., Dibitetto,D., De Gregorio,G., Eapen,V.V., Rawal,C.C., Lazzaro,F., Tsabar,M., Marini,F., Haber,J.E. and Pellicioli,A. (2015) Functional interplay between the 53BP1-ortholog Rad9 and the Mre11 complex regulates resection, end-tethering and repair of a double-strand break. *PLos Genet.*, **11**, e1004928.
46. Lee,S.E., Moore,J.K., Holmes,A., Umezu,K., Kolodner,R.D. and Haber,J.E. (1998) Saccharomyces Ku70, mre11/rad50 and RPA proteins regulate adaptation to G2/M arrest after DNA damage. *Cell*, **94**, 399–409.
47. Hoch,N.C., Chen,E.S., Buckland,R., Wang,S.C., Fazio,A., Hammet,A., Pellicioli,A., Chabes,A., Tsai,M.D. and Heierhorst,J. (2013) Molecular basis of the essential s phase function of the rad53 checkpoint kinase. *Mol. Cell Biol.*, **33**, 3202–3213.
48. Ira,G., Malkova,A., Liberi,G., Foiani,M. and Haber,J.E. (2003) Srs2 and Sgs1-Top3 suppress crossovers during double-strand break repair in yeast. *Cell*, **115**, 401–411.
49. Mazon,G. and Symington,L.S. (2013) Mph1 and Mus81-Mms4 prevent aberrant processing of mitotic recombination intermediates. *Mol. Cell*, **52**, 63–74.
50. Ivanov,E.L., Sugawara,N., Fishman-Lobell,J. and Haber,J.E. (1996) Genetic requirements for the single-strand annealing pathway of double-strand break repair in Saccharomyces cerevisiae. *Genetics*, **142**, 693–704.
51. Hegnauer,A.M., Hustedt,N., Shimada,K., Pike,B.L., Vogel,M., Amsler,P., Rubin,S.M., van Leeuwen,F., Guenole,A., van Attikum,H. *et al.* (2012) An N-terminal acidic region of Sgs1 interacts with Rpa70 and recruits Rad53 kinase to stalled forks. *EMBO J.*, **31**, 3768–3783.
52. Nielsen,I., Bentsen,I.B., Andersen,A.H., Gasser,S.M. and Bjergbaek,L. (2013) A Rad53 independent function of Rad9 becomes crucial for genome maintenance in the absence of the Recq helicase Sgs1. *PLoS One*, **8**, e81015.
53. Gravel,S., Chapman,J.R., Magill,C. and Jackson,S.P. (2008) DNA helicases Sgs1 and BLM promote DNA double-strand break resection. *Genes Dev.*, **22**, 2767–2772.
54. Granata,M., Lazzaro,F., Novarina,D., Panigada,D., Puddu,F., Abreu,C.M., Kumar,R., Grenon,M., Lowndes,N.F., Plevani,P. *et al.* (2010) Dynamics of Rad9 chromatin binding and checkpoint function are mediated by its dimerization and are cell cycle-regulated by CDK1 activity. *PLos Genet.*, **6**, e1001047.
55. Grenon,M., Costelloe,T., Jimeno,S., O'Shaughnessy,A., Fitzgerald,J., Zgheib,O., Degerth,L. and Lowndes,N.F. (2007) Docking onto chromatin via the Saccharomyces cerevisiae Rad9 Tudor domain. *Yeast*, **24**, 105–119.
56. Bork,P., Hofmann,K., Bucher,P., Neuwald,A.F., Altschul,S.F. and Koonin,E.V. (1997) A superfamily of conserved domains in DNA damage-responsive cell cycle checkpoint proteins. *FASEB J.*, **11**, 68–76.
57. Weinert,T.A. and Hartwell,L.H. (1988) The RAD9 gene controls the cell cycle response to DNA damage in Saccharomyces cerevisiae. *Science*, **241**, 317–322.
58. Toh,G.W., O'Shaughnessy,A.M., Jimeno,S., Dobbie,I.M., Grenon,M., Maffini,S., O'Rorke,A. and Lowndes,N.F. (2006) Histone H2A phosphorylation and H3 methylation are required for a novel Rad9 DSB repair function following checkpoint activation. *DNA Repair (Amst.)*, **5**, 693–703.
59. Huyen,Y., Zgheib,O., Ditullio,R.A. Jr, Gorgoulis,V.G., Zacharatos,P., Petty,T.J., Sheston,E.A., Mellert,H.S., Stavridi,E.S. and Halazonetis,T.D. (2004) Methylated lysine 79 of histone H3 targets 53BP1 to DNA double-strand breaks. *Nature*, **432**, 406–411.
60. Travesa,A., Duch,A. and Quintana,D.G. (2008) Distinct phosphatases mediate the deactivation of the DNA damage checkpoint kinase Rad53. *J. Biol. Chem.*, **283**, 17123–17130.
61. Jinks-Robertson,S., Michelitch,M. and Ramcharan,S. (1993) Substrate length requirements for efficient mitotic recombination in Saccharomyces cerevisiae. *Mol. Cell Biol.*, **13**, 3937–3950.
62. Bhargava,R., Onyango,D.O. and Stark,J.M. (2016) Regulation of single-strand annealing and its role in genome maintenance. *Trends Genet.*, **32**, 566–575.
63. Weinstock,D.M., Richardson,C.A., Elliott,B. and Jasin,M. (2006) Modeling oncogenic translocations: distinct roles for double-strand break repair pathways in translocation formation in mammalian cells. *DNA Repair (Amst.)*, **5**, 1065–1074.
64. Tutt,A., Bertwistle,D., Valentine,J., Gabriel,A., Swift,S., Ross,G., Griffin,C., Thacker,J. and Ashworth,A. (2001) Mutation in Brca2 stimulates error-prone homology-directed repair of DNA double-strand breaks occurring between repeated sequences. *EMBO J.*, **20**, 4704–4716.